


AD-A251 492		ION PAGE		Form Approved OMB No. 0704-0188	
Public gather collect Davis				page 1 hour per response, including the time for reviewing instructions, searching existing data sources, collection of information. Send comments regarding this burden estimate or any other aspect of this Washington Headquarters Services, Directorate for Information Operations and Reports, 1215 Jefferson nagement and Budget, Paperwork Reduction Project (0704-0188), Washington, DC 20503.	
1. AGENCY USE ONLY (Leave blank)		6/92		3. REPORT TYPE AND DATES COVERED TECHNICAL	
4. TITLE AND SUBTITLE SHALLOW WATER SEDIMENT PROPERTIES DERIVED FROM HIGH-FREQUENCY SHEAR AND INTERFACE WAVES				5. FUNDING NUMBERS ONR N00014-88-C-1238	
6. AUTHOR(S) JOHN EWING, JERRY A. CARTER, GEORGE H. SUTTON AND NOEL BARSTOW					
7. PERFORMING ORGANIZATION NAME(S) AND ADDRESS(ES) WOODS HOLE OCEANOGRAPHIC INSTITUTION WOODS HOLE, MA 02543				8. PERFORMING ORGANIZATION REPORT NUMBER WHOI CONTR. NONE	
9. SPONSORING/MONITORING AGENCY NAME(S) AND ADDRESS(ES) OFFICE OF NAVAL RESEARCH ENVIRONMENTAL SCIENCES DIRECTORATE ARLINGTON, VA 22217				10. SPONSORING/MONITORING AGENCY REPORT NUMBER	
11. SUPPLEMENTARY NOTES In citing this report in a bibliography, the reference given should be: JOURNAL OF GEOPHYSICAL RESEARCH 97(B4):4739-4762, 1992					
12a. DISTRIBUTION/AVAILABILITY STATEMENT APPROVED FOR PUBLIC RELEASE: DISTRIBUTION UNLIMITED				12b. DISTRIBUTION CODE DTIC ELECTE S A D JUN 16 1992	
13. ABSTRACT (Maximum 200 words) Low-frequency sound propagation in shallow water environments is not restricted to the water column but also involves the subbottom. Thus, as well as being important for geophysical description of the seabed, subbottom velocity/attenuation structure is essential input for predictive propagation models. To estimate this structure, bottom-mounted sources and receivers were used to make measurements of shear and compressional wave propagation in shallow water sediments of the continental shelf, usually where boreholes and high-resolution reflection profiles give substantial supporting geologic information about the subsurface. This colocation provides an opportunity to compare seismically determined estimates of physical properties of the seabed with the "ground truth" properties. Measurements were made in 1986 with source/detector offsets up to 200 m producing shear wave velocity versus depth profiles of the upper 30-50 m of the seabed (and P wave profiles to lesser depths). Measurements in 1988 were made with smaller source devices designed to emphasize higher frequencies and recorded by an array of 30 sensors spaced at 1-m intervals to improve spatial sampling and resolution of shallow structure. These investigations with shear waves have shown that significant lateral and vertical variations in the physical properties of the shallow seabed are common and are principally created by erosional and depositional processes associated with glacial cycles and sea level oscillations during the Quaternary. When the seabed structure is relatively uniform over the length of the profiles, the shear wave fields are well ordered, and the matching of the data with full waveform synthetics has been successful, producing velocity/attenuation models consistent with the subsurface lithology indicated by coring results. Both body waves and					
14. SUBJECT TERMS 1) SUBBOTTOM VELOCITY/ATTENUATION STRUCTURE 2) PREDICTIVE PROPAGATION MODELS 3) SHEAR AND COMPRESSED WAVE PROPAGATION				15. NUMBER OF PAGES - 23	
				16. PRICE CODE	
17. SECURITY CLASSIFICATION OF REPORT UNCLASSIFIED		18. SECURITY CLASSIFICATION OF THIS PAGE UNCLASSIFIED		19. SECURITY CLASSIFICATION OF ABSTRACT UNCLASSIFIED	
20. LIMITATION OF ABSTRACT					

Shallow Water Sediment Properties Derived From High-Frequency Shear and Interface Waves

JOHN EWING

Woods Hole Oceanographic Institution, Woods Hole, Massachusetts

JERRY A. CARTER,¹ GEORGE H. SUTTON,² AND NOEL BARSTOW³

Rondout Associates, Incorporated, Stone Ridge, New York

Low-frequency sound propagation in shallow water environments is not restricted to the water column but also involves the subbottom. Thus, as well as being important for geophysical description of the seabed, subbottom velocity/attenuation structure is essential input for predictive propagation models. To estimate this structure, bottom-mounted sources and receivers were used to make measurements of shear and compressional wave propagation in shallow water sediments of the continental shelf, usually where boreholes and high-resolution reflection profiles give substantial supporting geologic information about the subsurface. This collocation provides an opportunity to compare seismically determined estimates of physical properties of the seabed with the "ground truth" properties. Measurements were made in 1986 with source/detector offsets up to 200 m producing shear wave velocity versus depth profiles of the upper 30–50 m of the seabed (and *P* wave profiles to lesser depths). Measurements in 1988 were made with smaller source devices designed to emphasize higher frequencies and recorded by an array of 30 sensors spaced at 1-m intervals to improve spatial sampling and resolution of shallow structure. These investigations with shear waves have shown that significant lateral and vertical variations in the physical properties of the shallow seabed are common and are principally created by erosional and depositional processes associated with glacial cycles and sea level oscillations during the Quaternary. When the seabed structure is relatively uniform over the length of the profiles, the shear wave fields are well ordered, and the matching of the data with full waveform synthetics has been successful, producing velocity/attenuation models consistent with the subsurface lithology indicated by coring results. Both body waves and interface waves have been modeled for velocity/attenuation as a function of depth with the aid of synthetic seismograms and other analytical techniques. Some results give strong evidence of anisotropy and lateral heterogeneity in shear velocity of the upper 5–10 m of sediments and of extremely high velocity gradients in the topmost 1–2 m, possibly exceeding 30 s^{-1} .

INTRODUCTION

Modern models of acoustic propagation in coastal regions have demonstrated clearly the need for knowledge of the subbottom shear velocity and absorption, as functions of depth, to predict the propagation loss adequately [Akal, 1980; Ferla *et al.*, 1980; McDaniel and Beebe, 1980; Vidmar and Koch, 1986; Beebe and Holland, 1986; Hughes *et al.*, 1990]. These authors note the importance of bottom rigidity as a low-frequency loss mechanism in model/data comparisons and the general lack of adequate shear wave environmental data. Akal [1980] emphasizes the importance of seafloor-dependent propagation losses at lower frequencies and the existence of an optimum (minimum loss) frequency resulting from the interaction of the different major loss mechanisms. Optimum frequency is dependent upon water depth and upon seafloor geoaoustic characteristics. A range of optimum frequencies from about 50 to 800 Hz was observed for sediment ranging from clay to coarse sand; greater water depth generally produces lower frequencies for

all sediment types. Hughes *et al.* [1990] explained unexpectedly high propagation loss observed in some shallow water areas as being caused by shear wave absorption within thin sediment cover over a hard rock subbottom.

In addition to their importance for complete propagation models, shear velocities are much more sensitive than compressional velocities to structures and lithologies of the subbottom sediments: shear velocities vary by orders of magnitude whereas compressional velocities vary by less than a factor of 2. The shear velocity of unconsolidated and semiconsolidated sediments is less than that of sound in water and ranges down to a few tens of meters per second for high-porosity sediments. The low shear velocity produces downward refraction and makes "total" reflection of a hydroacoustic wave impossible and some energy generally will be converted to shear in the bottom. The conversion efficiency depends upon angle of incidence and impedance contrast. Vidmar [1980a, b] investigated the dependence of bottom reflection loss on the geoaoustic parameters of solid sediments and found: shear and compressional velocities in both the sediments and substrate are clearly important parameters; sediment shear and compressional gradients are also important; shear and compressional attenuations are important at certain frequencies and layer thicknesses. Stern *et al.* [1983] have extended this work utilizing the Biot [1962] and Stoll [1980] model for dissipative, water-saturated sediments. Earlier, Hawker [1979] demonstrated the importance

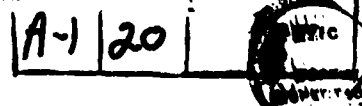
¹Now at Center for Seismic Studies, SAIC, Arlington, Virginia.

²Now at Woods Hole Oceanographic Institution, Woods Hole, Massachusetts.

³Now at Piermont, New York.

Copyright 1992 by the American Geophysical Union.

Paper number 92JB00180.
0148-0227/92/92JB-00180\$05.00



of conversion to Stoneley/Scholte interface waves, whose properties depend strongly on subbottom shear velocities, as a loss mechanism in plane wave reflection problems. Hamilton [1976a, b, 1979] has compiled the most complete summaries of existing data on shear velocities, V_p - V_s ratios (Poisson's ratios), and shear attenuation in marine sediments and rocks. These data are included in his geoacoustic models of the seafloor [Hamilton, 1980]. Milholland et al. [1980] produced geoacoustic models for deep-sea carbonate sediments, based on ultrasonic measurements on JOIDES cores, that include shear velocity and shear anisotropy versus depth.

Very few in situ data exist on shear velocity and attenuation in the upper tens of meters of bottom sediment. Most shear velocity information has been derived from interpretation of low-frequency Stoneley/Scholte interface waves generated by explosions on or near the bottom with frequencies less than 100 Hz [Bucker et al., 1964; Davies, 1965; Essen, 1980; Rauch, 1980, 1986; Schirmer, 1980; Schmalfeldt, 1986; Snoek et al., 1986; Jensen and Schmidt, 1986; Sauter et al., 1986; Schreiner and Dorman, 1990]. These waves involve both compressional and shear energy, and amplitudes fall off exponentially with distance above and below the bottom. They are dispersive if the velocities change away from the interface and can be considered to be a particular solution of the general Rayleigh wave problem.

The possible effects of anisotropy and lateral heterogeneity on propagation loss are poorly known. Most marine sediments are expected to exhibit transverse isotropy, which is a form of anisotropy with a single, vertical axis of symmetry [Fryer and Miller, 1986]. This can result from intrinsic anisotropy of gravitationally oriented particles, or pore spaces, or (more likely) from variations in sediment properties with depth at a scale small compared to a wavelength [Milholland et al., 1980]. Most observed (and imagined) situations produce higher compressional wave speed in the horizontal plane than in the vertical direction: horizontally propagating, horizontally polarized shear is faster than horizontally propagating, vertically polarized, or vertically propagating shear. The observation of both horizontally polarized (SH) and vertically polarized (SV) shear along with compressional waves permits the estimation of the five independent elastic parameters of transverse isotropy [Berge et al., 1991a]. Berge [1991] and Berge et al. [1991b] demonstrated that in transversely isotropic sediments serious errors in shear wave interval velocity can result from conventional interpretation of seismic reflection stacking velocities. "Shear wave splitting," i.e., different travel times between a given source and receiver of shear waves with orthogonal polarization, is a classical indication of seismic anisotropy [Crampin, 1985]. Anisotropy without a vertical axis of symmetry and lateral heterogeneity can be caused by, e.g., azimuthal variations in sedimentation, lithification, and erosion. Obviously, complete characterization of the most general case is quite difficult. However, the importance of these conditions on propagation can be estimated and predicted from the results of appropriate experiments in different environments.

Despite anticipated problems with source/sensor coupling to the seafloor, we have chosen to include the measurement of SH and Love wave energy which, unlike P/SV energy, is decoupled from P at impedance boundaries in an isotropic medium where properties vary only with depth. Therefore,

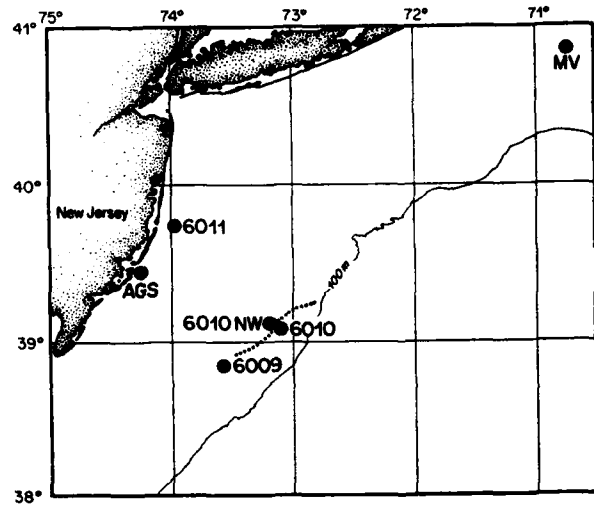


Fig. 1. Map of experiment locations: Atlantic Generating Station (AGS) drilling sites; 6009-6011, AMCOR drill sites [Hathaway et al., 1976]; MV, site south of Martha's Vineyard. Dotted line shows location of a boundary between two sedimentary regimes discussed later.

sources were developed to produce both longitudinally polarized and transversely polarized energy. Three orthogonal components of motion and pressure were recorded, generally along linear profiles. Each of the four components produced data that provide unique information on wave type, velocity/attenuation structure, scattering, lateral heterogeneity, instrument-bottom coupling (possible signal distortion) and anisotropy.

EQUIPMENT AND FIELD TECHNIQUES

Data for this study were collected during two different field seasons: summer 1986 and summer 1988. Figure 1 shows the geographic location of the study areas at Atlantic Margin Coring Project (AMCOR) drill site 6011 on the inner shelf, AMCOR sites 6009, 6010, and 6010 NW on the outer shelf, at the Atlantic Generating Station (AGS) drill sites near Atlantic City, New Jersey, and at a site south of Martha's Vineyard (MV). Although different equipment was used for signal generation and recording during the two cruises, the type of data was the same: artificially generated short-range seismic body and interface waves. Seismic waves generated in the sediments by a controlled shear wave source sled (which also generated compressional waves) were recorded at distances ranging from 1 to 200 m by geophones, accelerometers, hydrophones.

The shear sled design, used in the 1986 experiments and illustrated in Figure 2a, is similar conceptually to one developed at the University of Kiel [Gehrmann et al., 1984; Meissner et al., 1985]. The approximate dimensions are 2 m in length, 1.5 m in width, and 1.5 m in height, including the troika frame which insures upright attitude on the seafloor. Bolt 10 cu. in. (164 cc) airguns, modified to operate in dirty water and mounted in side-by-side horizontal steel cylinders, act as cannons to provide oppositely directed horizontal thrusts. The sled weighs about 300 kg and has fore-to-aft rails on its base to provide coupling to the seafloor. Alternate firing of the airgun-powered port and starboard cannons

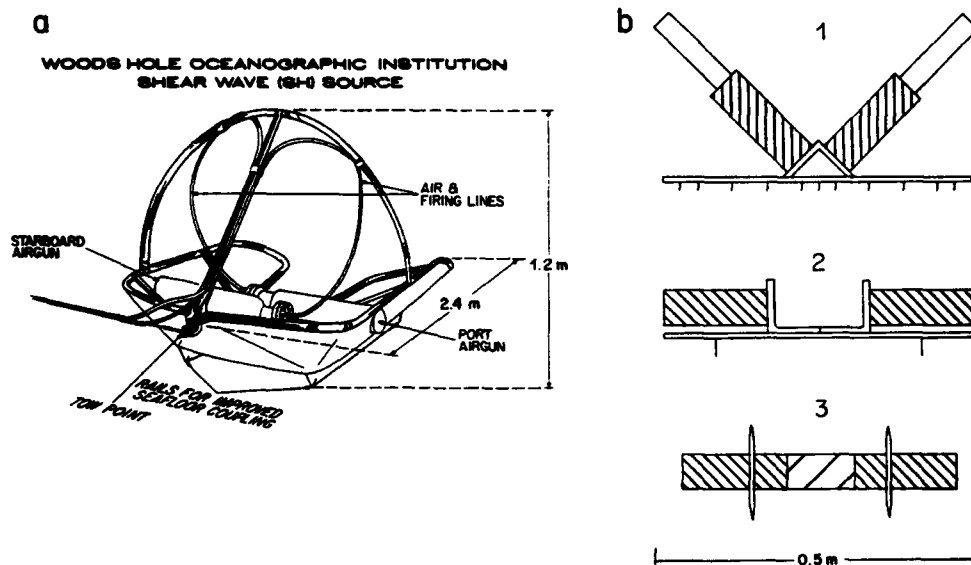


Fig. 2. Horizontal shear wave sources: (a) air gun shear sled; (b) three versions of shotgun shear sources (port-starboard cross-sectional view).

produces alternately polarized SH excitation: similarly polarized P and SV waves are also generated with each shot. Subtraction or addition of the data from the port and starboard shot pair then gives the desired result of producing primarily SH data with the subtraction and primarily P/SV data with the addition.

Figure 2b shows three versions of source configuration used in 1988. Sources 1 and 2 have cannons mounted on toboggan sleds. The source 3 design is cylindrical with back-to-back cannons and discs for coupling. All utilized electrically fired shotgun shells to produce the seismic excitation with port and starboard cannons, conceptually similar to the air gun-powered sled used in the 1986 work. In sources 2 and 3 the cannons are mounted horizontally; in source 1 they are mounted 45° to the horizontal with the view that coupling to the seabed would be improved by a downward component of thrust. This configuration compensated partially for the light weight and shallow coupling rails, thus increasing SH excitation. As anticipated, the shotgun shell sources produced much higher frequency signals (between 20 and 50 Hz) than the heavier air gun shear sled, which produced energy mainly in the 10- to 25-Hz band. However, the ratio of transverse to longitudinal energy produced by the small sources was disappointing. Apparently, the greater weight of the air gun sled was an important factor in coupling SH energy more efficiently.

The sensor package used in 1986 contained three 4.5-Hz gimballed orthogonal geophones and a hydrophone mounted on a toboggan sled which, like the source sled, was of troika design. The geophones were immersed in a viscous oil for mechanical damping. Sensors on the receiver sled were preamplified and hard-wired to the surface: the electrical cable served also to tow the sled. Aboard ship, the analog data were fed to a 16-bit digitizer and later displayed as seismogram sections after appropriate range adjustments, amplitude scaling, and filtering. Digitization intervals were 1 ms for the hydrophone and 4 ms for geophones. The sketch in Figure 3 shows the ship and sleds positioned for beginning

the recording of a profile. The deployment procedures are (1) to anchor the ship with 300–400 m of anchor cable payed out, (2) while hauling in anchor cable, to deploy the receiver sled and cable on bottom, towing the sled a short distance for proper orientation and (3) to deploy the source sled and tow it for orientation while paying out the necessary additional receiver cable. In recording the profile, the receiver sled is pulled (usually in increments of 4–8 m) toward the source sled. At each range, the receiver cable is slacked, and one or more shots are fired with each cannon. The source sled remains in the same position throughout the profile unless adverse wind or current changes occur. Misalignment of the horizontal components on the toboggan can be corrected (assuming negligible lateral refraction) by mathematically rotating the data to minimize the longitudinal signals on the transverse component. Misorientation of the source sled merely reduces the SH amplitudes. In discussion of the data from these experiments we designate the sensor components as R , T , V , and P for radial-horizontal, transverse-horizontal, vertical, and pressure, respectively.

Experience from the 1986 cruise indicated that better resolution of the uppermost sediment structure, where velocity gradients are generally greatest, requires higher-frequency data and closer, more accurate spacing of sources and receivers. This, in turn, requires smaller source and receiver elements. Thus significant modifications in the recording scheme were made prior to the 1988 measurements. Instead of using a single receiving package to record data from a large number of shots at different ranges, we converted to receiver arrays with source devices fastened to the array cable, at either or both ends of the active section. This configuration generally provided a fixed source-receiver geometry and uniform spatial sampling.

An accelerometer (ladder) array [Harris and Sutton, 1988] was the principal receiving system for the 1988 measurements. The array contains 30 receiving nodes spaced at 1-m intervals (Figure 4). Each node consists of a plastic disc approximately 40 cm in diameter and 6 cm thick containing

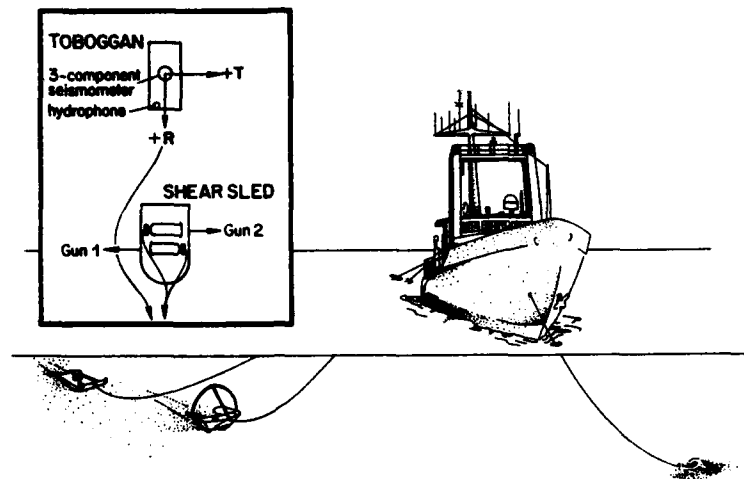


Fig. 3. Schematic of deployment of *SH* shear sled and toboggan. Note that the ground moves opposite to the direction of the expelled air, which is shown by the arrows.

a hydrophone, three orthogonal accelerometers, and a vertical direction sensor. The discs are held between the sides (wire ropes) and rungs (stiff plastic tubing) of the ladder by short lengths of chain with enough slack to isolate the discs

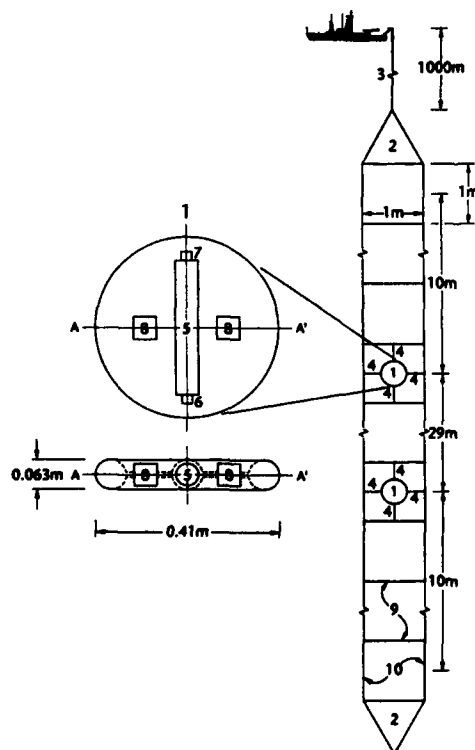


Fig. 4. Thirty node digital accelerometer/hydrophone (ladder) array: 1, sensor puck, fiberglass covered, resembling four-quadrant waffle; 2, end triangle housing A/D and electro-optical converters; 3, armored electro-optical cable; 4, loose chain coupling puck to array; 5, three-component accelerometer pressure case; 6, hydrophone; 7, electrical connector; 8, balance weight; 9, rigid cross members; and 10, flexible electrical and strain cables in split fire hose.

from ladder vibration while maintaining their orientation. The sources are similarly mounted at one or both ends of the array. Signals from the sensors are preamplified, transmitted electrically to one of two amplifier and A/D converter units at either end of the array, and then transmitted via optical fiber to the ship for recording. The 16-bit A/D converters digitize each hydrophone output at 0.5-ms intervals, and each accelerometer output at 2-ms intervals. Preamplifier gains can be adjusted in four groups along the array to compensate for spreading loss and attenuation. A serious effort was made to meet the requirements for good coupling to the bottom: sensor symmetry is maximized, coupling to the water is minimized, and density is matched to the sediment [Sutton and Duennebie, 1987]. Calculations, using equations of Sutton and Duennebie [1987] and Hsieh [1962], indicate that both horizontal and vertical bottom motions should be faithfully recorded for frequencies below about 50 Hz. Ship-to-array communication via the optical cable permits firing the shotgun shells in synchronization with data recording.

A backup 10-node geophone array containing 10-Hz R and T components, along with four hydrophone nodes, was used for some measurements. Shotgun shell sources were attached to the array cable 2 m and/or 8 m ahead of the nearest geophone node of the receiver array. When two sources were used a 2-m sampling interval was provided over a range from 2 to 40 m of source-receiver spread. Although some useful results were obtained with this array, a poor matching of the geophones with the recording amplifiers (the same as those used with the ladder array) restricted the dynamic range and usually caused overloading of the data from the near traces. Overloading of near trace data was also difficult to avoid with the ladder array due to the large amplitude changes caused by ray divergence.

SEISMIC WAVEFORM MODELING

The objective of our data analysis is to obtain detailed models of the shear wave properties of the upper few tens of meters of sediment by matching recorded data with full

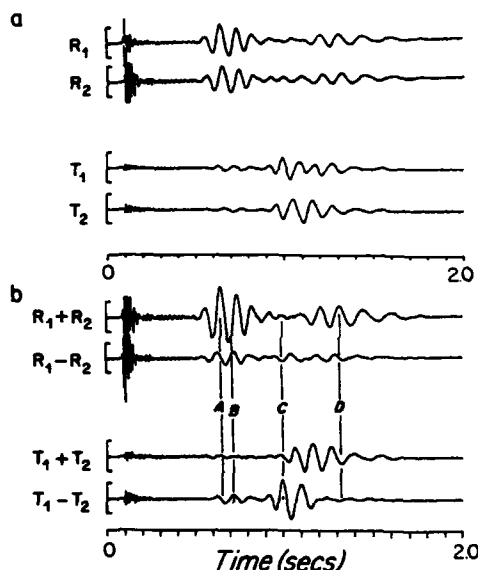


Fig. 5. AGS profile 1819 shots 27 and 28 alternate pair at 115 m range. (a) Mostly longitudinal R components and mostly transverse T components show quite different signals. R shows large, high-frequency early water wave arrival and in-phase later arrivals; T shows small, high-frequency early water wave arrival and much out-of-phase later signal. (b) Sums and differences for the R and T records shown in Figure 5a. $R_1 + R_2$ should be mostly longitudinal (P/SV/LR) energy. $T_1 - T_2$ should be mostly transverse (SH/LQ) energy. The other two traces, $R_1 - R_2$ and $T_1 + T_2$ should have small amplitudes. Lines A, D and B, C indicate times of maxima of longitudinal and transverse energy, respectively. The large "error" signal between C and D on the $T_1 + T_2$ trace is discussed in the text.

waveform synthetic seismograms. The starting point of the seismogram matching is to condition the raw data. At each source-receiver range, data from shot pairs recorded by the seismometers were summed for the R and V components, and subtracted for the T component in order to enhance the P/SV/LR energy in the R and V data and the SH/LQ energy in the T data. Figure 5 shows results of the combination of port-starboard shot pairs at 115-m range. When the geophone toboggan is oriented approximately toward the source (either initially or by mathematically rotating the horizontal data to minimize the high-velocity, longitudinal data on T) and the two sources are well matched, $R_1 + R_2$ (sum of radial seismograms generated by sources 1 and 2) should be the longitudinal (radial) component of P/SV/LR Stoneley-Scholte, and $T_1 - T_2$ should be transverse, i.e., SH/LQ. In that situation $R_1 - R_2$ and $T_1 + T_2$ should be relatively small; a large signal on $R_1 - R_2$ or $T_1 + T_2$ indicates some violation of the assumptions concerning the instrumentation or different amounts of lateral refraction for longitudinal and transverse modes.

Times A and D in Figure 5 indicate maxima on the $R_1 + R_2$ trace and are almost certainly longitudinal arrivals. The relatively large error trace, $R_1 - R_2$, is about 90° out of phase with $R_1 + R_2$. Times B and C indicate maxima on the $T_1 - T_2$ trace. Time C represents a strong transverse arrival. B also probably is a transverse arrival since the error trace $T_1 + T_2$ at that time is small. The strong signal between C and D on error trace $T_1 + T_2$ looks like longitudinal motion arriving mostly in the T (almost transverse) direction. This

arrival appears to result from an imperfection in the source sled used in the 1986 profiles. From inspection of the sketch of the shear sled in Figures 2 and 3 we see that while guns 1 and 2 produce forces in opposite directions, they both produce a counterclockwise torque on the bottom. Thus summed traces should include the contribution of the torque source. In addition, we expect that the torque source will have a node in the radiation pattern in the vertical direction, while the lateral force sources do not, resulting in an emphasis in the lower-velocity, shallow propagation as observed in the $T_1 + T_2$ trace of Figure 5 [Dorn, 1984]. The sources used in 1988 (Figure 2b) should not exhibit this behavior. However, it is typical that summed transverse traces contain a significant amount of energy resulting from lateral refraction, scattering, or some amount of azimuthally dependent anisotropy. In some cases using an air gun suspended near the bottom, which should have produced P/SV modes only, a great deal of transverse motion is present, sometimes increasing relative to P/SV with range (to be discussed later). It appears that conversion from longitudinal (P/SV) to transverse (SH) motion provides a significant loss mechanism not generally considered in calculations of propagation loss [Carter et al., 1987].

In the next step of data analysis, careful observations of the body wave arrival times from the seismic data are modeled for velocity structure using ray trace methods. Velocities estimated from densities and shear moduli calculated from available core data are used to supplement the seismic data for a preliminary velocity-depth model. If a dense sampling of cores is available, an indication of the lateral heterogeneity of the area is also obtained. At this point a fairly good model of the shear velocity has been obtained. To derive models for the attenuation, scattering, and anisotropy, however, the amplitude and phase relations as well as the arrival times of all three components of motion and pressure should be considered. We do this by matching waveform data to full waveform synthetic seismograms based on the "locked mode" technique developed by Harvey [1981]. The models are limited to isotropic horizontal constant-velocity layers and each layer can be assigned frequency-dependent Q for compressional and shear energy. Gradients are approximated by thin layers with small velocity changes. In addition to modeling the body waves, full waveform synthetic seismograms model the interface waves, both vertically and horizontally polarized, which are sensitive indicators of the attenuation properties of the upper few meters of sediment. Their amplitudes relative to other arrivals, and phase and group velocities, are also valuable for refining the velocity models derived from ray tracing. The maximum phase velocity included in the calculations of the synthetics is usually set at 500 m/s in order to eliminate compressional waves (and high phase velocity reflections from the high velocity layer at the base of the model that is required by the Harvey method). The phase velocity cutoff was increased to 1000 m/s when shear velocities near 500 m/s were involved in the model. The locked mode technique used does not model anisotropy. However, a medium that is vertically transversely isotropic (anisotropy with a vertical axis of symmetry) can be recognized by the differences between the best model for the P/SV data and best model for the SH data [Berge et al., 1991a].

The configuration of the shear source sleds requires that different source functions be used for the vertically polarized

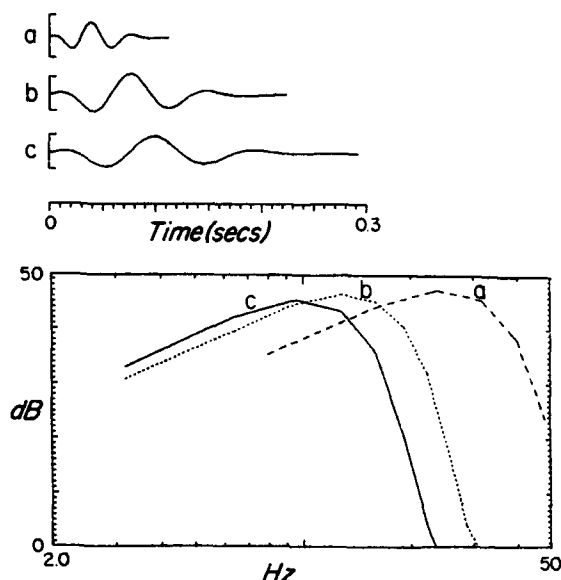


Fig. 6. Time series and spectra used to produce the synthetic seismograms. Spectra *a* and *b* were used for *SH* synthetics for 1988 and 1986, respectively; *c* was used for 1986 *P/SV* synthetics. The spectrum for 1988 *P/SV* source was centered at 20 Hz, not shown.

synthetics (*P/SV*) and the horizontally polarized synthetics (*SH*). *P/SV* energy is generated from the explosion in the water column by either the air gun or the shotgun shell, and thus the *P/SV* source is modeled as an impulsive explosion in the water column 10 cm above the sediment. The *SH* energy transferred to the sediments by the runners of the source sled is modeled as a set of five horizontal force vectors 3 cm below the water/sediment interface. The vectors are oriented perpendicular to and located at 0.25-m intervals along the profile line. The synthetics are computed in ground velocity up to a frequency of 25 Hz for comparison to the 1986 data and in ground acceleration up to 50 Hz for comparison to the 1988 data using the appropriate impulsive source function described above. The final step is to convolve the synthetics with a causal band-limited function representative of the source. For the 1986 *P/SV* synthetics this function was chosen to have a 10-Hz center frequency, and for the 1988 *P/SV* synthetics a 20-Hz center frequency was used. The *SH* center frequencies used are slightly higher than the *P/SV* center frequencies, 13 and 24 Hz for the 1986 and 1988 synthetics, respectively. The spectra and time series for the band-limiting functions used in the convolutions are shown in Figure 6.

RESULTS

AMCOR 6011

Five shear wave profiles were recorded in the vicinity of AMCOR site 6011 (Figure 7a). For profiles 2509 and 2520 the air gun shear sled and toboggan receiver sled were used. Profile 2408 was also recorded with the toboggan sled and with a standard air gun suspended near the seafloor as the source. The shotgun source sleds (Figure 2b, 1 and 2) and the 1988 geophone array were used for profiles A and B. Results from these two profiles were nearly identical, so only

profile B is discussed. A high frequency, 1–3 kHz, reflection profile recorded along a line through the drill site is shown in Figure 7b. Stratigraphic and lithologic data from the AMCOR borehole [Hathaway et al., 1976] are summarized in Figure 7c.

Figure 8 shows 15-Hz low-pass-filtered record sections of R, T, and V signals from sums (R, V) and differences (T) of port-starboard pairs of shots for profiles 2509 and 2520, which cross each other. Since it is the shorter profile, only the T component data for profile 2520 are shown, but the R and V data in the two profiles are equally comparable. The apparent difference between the T data in profiles 2509 and 2520 stems almost entirely from the closer trace spacing and concomitant lower gain used in 2520 to reduce trace overlap. The radial and vertical traces show first *SV* arrivals with phase velocities near 262 and 324 m/s at ranges of 0–50 and 50–178 m, respectively. Later arrivals are interface waves with a group velocity of 140 m/s and phase velocity of 200 m/s. The record section of the T shot pairs produces a clear *SH*/Love wave trace as anticipated, but with a group velocity of 170 m/s and a phase velocity of 217 m/s. There is little energy found in either the V or R data near the group velocity of the Love wave. Also shown in Figure 8 are the matching synthetic seismograms generated from our best models for this area. In general, the fit of the arrival times, amplitudes, and phases between the data and the synthetics is good for all three components of both profiles. The density and shear wave *Q* are adjusted so that the relative amplitudes between the R and V synthetics match the data and so that the synthetic seismogram amplitudes attenuate appropriately with distance. The most obvious misfit is the significant energy decrease at the beginning of the refracted *SH* arrival and the Love wave at ranges beyond 117 m in the T component data of profile 2509. Perfect fits of the amplitudes from trace to trace cannot be expected as each data trace represents a different set of shot pairs. That the amplitudes are as well behaved as they are is a testament to the repeatability of the source and coupling of the toboggan receiver package to the bottom.

The best fit of synthetic seismograms to the data requires that different models be used to fit the T data and the R/V data. The T model has 5% higher velocities than the R/V model in the upper 15 m of seabed. Both models, the stair steps, are shown in Figure 9 (only the longitudinal model parameters are listed in Table 1). They are roughly characterized by an average gradient of about 10 s^{-1} above 15 m depth and a gradient of 1.6 s^{-1} at greater depth. The fact that velocities in the silty clay layer are higher in the T model than in the R/V model is consistent with a transversely isotropic medium (with a vertical axis of symmetry). As mentioned in the introduction, in a medium with thin horizontal layers of variable rigidity, horizontally propagating, horizontally polarized shear waves travel faster than vertically polarized waves [Berge et al., 1991a]. A more complete treatment of the anisotropic properties of this data set is given by Berge et al., who have modeled profiles 2509 and 2520 using a synthetic seismogram program developed by Mallick and Frazer [1988, 1990] that allows general anisotropy.

The starting model, derived by ray tracing is shown in Figure 9 and, although it is similar to the final model, it did not produce an acceptable data/synthetics match. For example, in the final model a thin low velocity zone in the silty

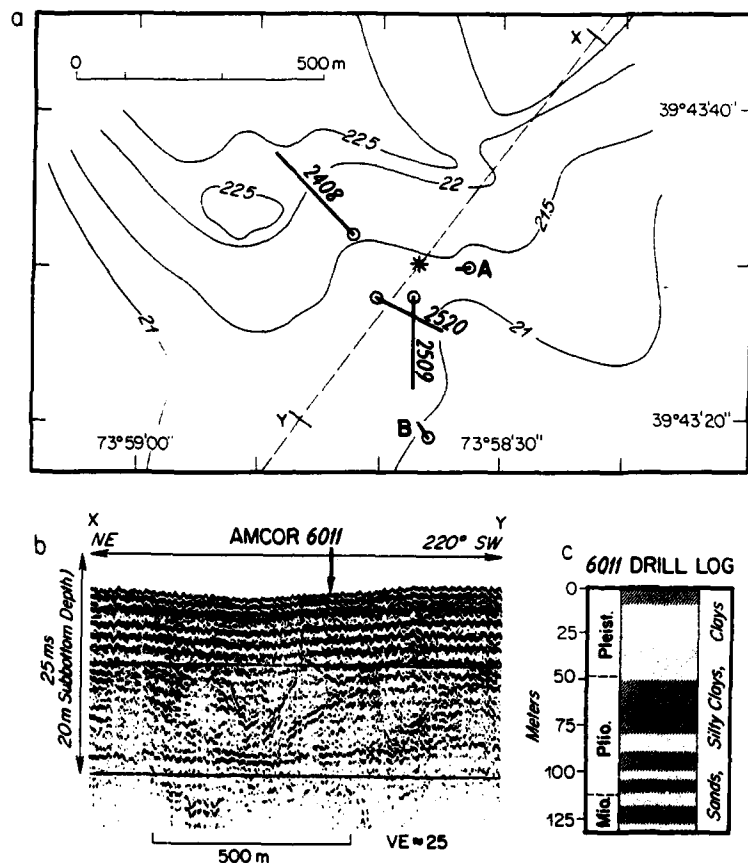


Fig. 7. (a) Map of AMCOR 6011 area; bathymetric contours in meters. Asterisk locates drill site. Open circles and line segments show measurement locations: the circles are at the source locations. Profiles 2408-2520 were shot in 1986; profiles A and B were shot in 1988. (b) Reflection profile along NE-SW dashed line through the drill site shows evidence of channel erosion and refilling. (c) Drilling results [Hathaway et al., 1976]. Stippling represents coarser sediment; hatching represents finer sediment.

clay layer is required to match the phase velocity of the Stoneley/Scholte waves. Neither this model feature nor the evidence for transverse isotropy could have been determined by ray tracing. The ray trace model does, nevertheless, provide a useful starting point for full waveform iterative modeling. The relatively high frequency data (25–30 Hz) recorded in profile B (Figure 9 inset) provided good constraint on the velocity structure to a depth of ~7 m. The longer range data of profile 2509 provided information on the velocity structure below 7 m. Also shown in Figure 9 are two velocity models derived by dispersion analysis and waveform modeling (SAFARI) of other seismic profiles near site 6011 [Stoll, 1989; Stoll et al., 1991]. There are obvious discrepancies, but perfect agreement between two measurements at different locations in this geologically complex area should not be expected, particularly in the 7- to 15-m depths range where the sedimentary section has obviously been reworked (Figure 7b). Rajan and Howitt [1991] obtained a velocity model from inversion of *SH* data from our profile 2509 (AMCOR site 6011), using multiple filter analysis of a single record at 61 m range to determine group velocity dispersion of the fundamental Love wave. The velocity model thus derived is also shown in Figure 9. Frequencies between 4 and 10 Hz were used, which they considered to

provide best constraint of the velocity model in the upper 20 m. Their model velocities are lower than ours by up to 74 m/s above 4-m depth, higher than ours by ~25 m/s between 4 and 8 m, and again lower by 25–40 m/s between 8 and 10 m. We have no explanation for this discrepancy except that their model is based on an average over 61 m range and ours is based on the entire record section with ranges out to 178 m.

The evidence of channel cut and fill seems to be at least partially contradictory to the observation made earlier that the 2509 and 2520 data indicate transverse isotropy above 15-m depth. Although the reflection profile shows the upper 6–8 m to be horizontally bedded, and thus consistent with transverse isotropy, the section between the horizontal bedding and a regional reflector at ~15 m below seafloor clearly is not laterally homogeneous for 1.5–3.0 kHz compressional wave imaging frequencies. It would appear that either the transverse isotropy is limited to the upper 6–8 m or that the area has been the site of a succession of channels, or a migrating channel, all of which have been filled with horizontally bedded sediment, thus producing an overall fabric appropriate to conditions for transverse isotropy.

There is other evidence that the filled channel is, in fact, distinctly laterally inhomogeneous. Figure 10 shows the *V* and *T* data from profile 2408 (Figure 7), for which the source

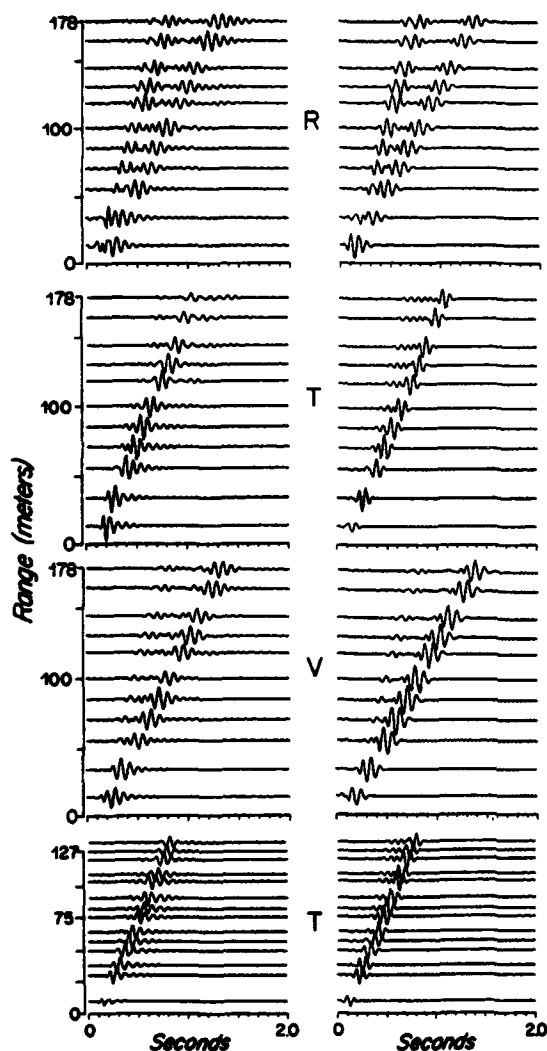


Fig. 8. Data (left) and synthetics (right) for R, T, and V components, respectively, at AMCOR 6011 profile 2509. At the bottom are T component data and synthetics for profile 2520. Note the closer trace spacing in profile 2520 and the concomitant lowering of gain to minimize trace overlap. Synthetics for both profiles are from the same model. In both data and synthetics, amplitudes are scaled proportional to range, and the V amplitudes are reduced by 0.5 relative to R.

was an air gun suspended near the seafloor. In a laterally homogeneous structure no transversely-polarized energy would be expected from this source. The T/V amplitudes ratios in Figure 10 were intentionally made to be ~ 1 by reducing vertical amplitude by a factor of 2.5. The range intervals between 46 and 175 m correspond closely to the amount of receiver cable pulled in between shots, which, along with mathematical rotation of the horizontal components, insures that the receivers were properly oriented relative to the source and that the energy received by the T component was not the result of receiver misalignment. Although poor coupling of the geophones to the seafloor might be partially responsible for the significant amplitudes observed in the T component, it is more likely that scattering and/or lateral refraction is the cause. The nonrandom spatial

coherence of the data supports this interpretation. The T energy arrives slightly after the V and reaches its maximum before the maximum of the V boundary wave. There are many examples of T energy having been generated by explosions, both in soil and in hard rock, and measured over ranges from meters to hundreds of kilometers [e.g., Kisslinger *et al.*, 1961; Gupta and Blandford, 1983]. Anisotropy in the propagation medium can also produce shear particle motion at an angle other than perpendicular to the propagation direction. However, we believe it is unlikely that the required type of anisotropy would be sufficiently strong in water-saturated, unconsolidated sediments to produce the observations.

Atlantic Generating Station (AGS)

Subsurface geologic data at the AGS were acquired by Dames and Moore as part of a Beach Haven site survey for the New Jersey Public Service Electric and Gas Company. Data interpretation was a cooperative project of Dames and Moore and the Marine Geology and Geophysics Laboratory of Atlantic Oceanographic and Meteorological Laboratories, National Oceanic and Atmospheric Administration. Seismic reflection surveys and vibracoring by Alpine Geophysical Associates [Miller and Dill, 1974] were components of the study. Several additional reflection lines recorded by Woods Hole Oceanographic Institute (WHOI) investigators in 1987

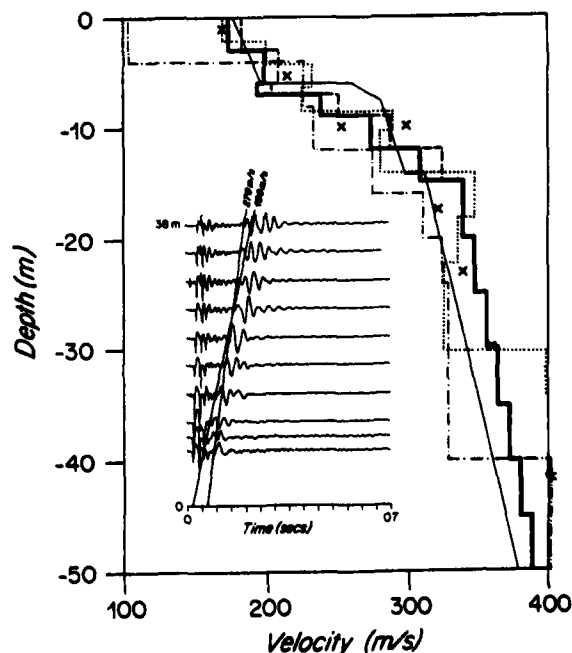


Fig. 9. Velocity models for AMCOR 6011. Broad solid line, P/SV; dashed line, SH; fine line, ray trace; crosses, Stoll (1989); dotted line, Stoll *et al.* [1991]; dot-dash line, [Rajan and Howitt (1991)]. These models are discussed in the text. The inset shows R component seismograms recorded at profile B (Figure 7) with the 1988 geophone array and shotgun source. These results along with those from profile A provided control of the shallow velocity structure for the ray trace model; the deep structure was determined by the data from profiles 2509 and 2520.

TABLE 1. Physical Parameters Used to Compute Full Waveform Synthetic Seismograms

Δh , m	V_p , m/s	V_s , m/s	ρ , kg/m ³	Q
<i>2509 Structure</i>				
021.0	1500	0	1000	0
3.0	1600	175	2000	40
3.0	1600	200	2000	40
1.0	1700	195	2000	40
2.0	1700	240	2000	40
3.0	1710	275	2000	40
3.0	1720	310	2000	40
5.0	1750	340	2000	40
5.0	1760	348	2000	40
5.0	1770	356	2000	40
5.0	1780	364	2000	40
5.0	1790	372	2000	40
5.0	1800	380	2000	40
5.0	1810	388	2000	40
505.0	1820	396	2000	40
<i>2113 Structure</i>				
12.000	1500	0	1000	0
0.464	1580	40	1600	20
0.464	1600	90	1800	20
0.464	1630	120	1900	20
0.464	1640	140	1900	20
0.464	1650	160	1900	20
0.464	1660	180	1900	20
1.616	1670	190	2000	40
2.0	1690	200	2000	40
2.0	1700	210	2000	40
2.0	1710	220	2000	40
4.0	1720	230	2000	40
1.0	1730	240	2000	40
3.0	1740	290	2000	40
15.0	1770	300	2000	40
15.0	1780	330	2000	40
15.0	1790	360	2000	40
334.0	1800	390	2000	40
<i>6009G Structure</i>				
1.12	1600	86	1600	40
5000.00	1820	209	1800	40
<i>1909 Structure</i>				
11.0	1500	0	1000	0
0.5	1600	90	2000	20
1.0	1640	180	2000	20
5.0	1640	140	2000	20
3.0	1640	135	2000	20
1.0	1640	240	2000	20
2.0	1640	250	2000	20
3.0	1640	260	2000	20
3.0	1640	270	2000	20
15.0	1680	300	2000	20
15.0	1700	330	2000	20
15.0	1720	360	2000	20
334.0	1750	450	2000	20
<i>2016 Structure</i>				
11	1500	0	1000	0
5	1680	200	1600	20
1	1800	500	2000	20
5	1640	140	1500	20
3	1720	240	1800	20
2	1730	250	1800	20
3	1740	260	1800	20
3	1750	270	1800	20
15	1760	300	1900	20
515	1810	510	2000	20
<i>2715 Structure</i>				
60	1500	0	1000	0
1	1600	104	1600	20
2	1680	219	1750	40

TABLE 1. (continued)

Δh , m	V_p , m/s	V_s , m/s	ρ , kg/m ³	Q
<i>2715 Structure (continued)</i>				
1	1700	301	1800	40
2	1710	329	1810	40
2	1720	335	1820	40
2	1730	342	1830	40
2	1740	348	1840	40
2	1750	355	1850	40
25	1690	274	1780	40
500	1760	361	1860	40

SV velocities are listed for 2509 structure; see Figure 9 for SH. Four additional velocity models and their synthetics are compared in Figure 25, and parameters for three "example" models are shown with the seismogram sections in Figures 28 and 29. Note that values of V_p and ρ are gross estimates, although they are within the range of admissible values for the particular lithologies and subsurface depths encountered. Test models have shown that within reasonable limits these parameters have little effect on the synthetic seismograms. The Q_s values do have significant effects and probably could be better determined by further model testing. As noted in the text, values of Q_s between 20 and 50 seem to be appropriate for these lithologies and seabed depths. A value of 1000 (effectively infinity) was used for Q_p .

(unpublished), at locations shown in Figure 11 have supported our interpretations of the subsurface structure.

Figure 11 is a bathymetric map of the AGS area showing locations of boreholes [Dames and Moore, 1974; Stahl et al., 1974] and our measurements. Straight-line segments with open circles at one end (the source location end) locate the seismic profiles to be discussed. The NE-SW closed contours (dotted lines) in the center of the diagram outline a large sand ridge with up to 7 m of surficial sand in the crest, tapering to zero thickness in the deeper area toward the NW. The approximate boundaries of a large buried channel underlying much of the AGS area are indicated by heavy sinuous lines. The double lines trending NW-SE locate three geologic cross sections that are based on the borehole data and on the WHOI reflection survey (thin dashed lines). These cross sections show details of the local geology and provide a framework within which to relate various structures and lithologies to features of the recorded shear wave seismogram sections.

Two profiles (1909 and 1809) recorded in the AGS area are located on the northwest flank of the sand ridge and within the buried channel (Figure 11). In the channel, approximately 10 m of Holocene sands, silts, clays and gravels disconformably overlie thick (>40 m) Tertiary sediments, which are predominantly sand interbedded with gravel and stiff clay. The basal portion of the channel fill is a soft, organic-rich clay, which was probably deposited during the regression of the mid-Wisconsin sea [Stahl et al., 1974]. Another nearby profile, 1819, crosses the western edge of the channel. Profiles 2113 and 2817 are outside the channel on the western bank, where the Tertiary sediments are overlain by Pleistocene clays, appreciably stiffer than the Holocene clay at comparable depth in the channel area. Two other profiles, 2016 and 2908, are located on the crest and southeastern flank of the sand ridge. The patterns of shear wave arrivals are quite different in these three regions. The following discussions will address these differences in the context of the aforementioned geologic cross sections.

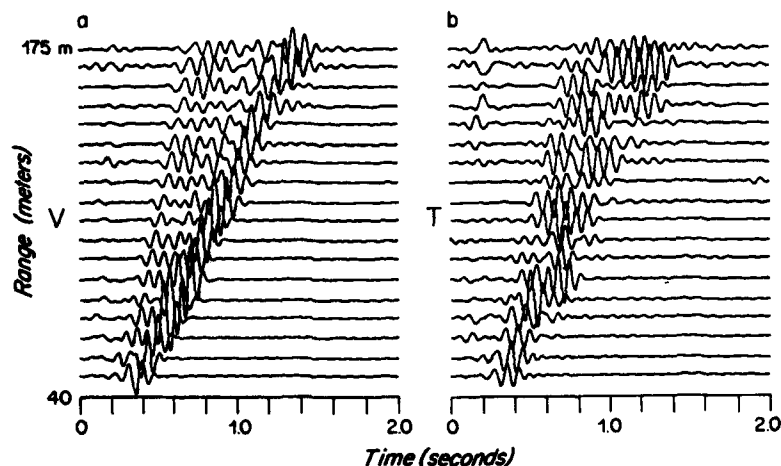


Fig. 10. (a) V and (b) T seismograms from profile 2408 (Figure 7) using air gun source suspended near bottom. This configuration should produce little or no signal from the T component unless the seabed is laterally heterogeneous, giving rise to scattering and/or lateral refraction. After amplification adjustments, the average T/V amplitude ratio is 0.4.

Cross Section A

As shown in Figure 11, cross section A closely parallels profile 1909 (in the channel) and extends northwestward almost to profile 2817 (out of the channel). Figure 12, modified from *Dames and Moore* [1974], shows the geologic structure and lithology along this section based on borehole and vibracore data. Also shown are the shear wave velocity values determined at 1909 and 2817. General descriptions of the various strata are given in the legend. The system of

strata numbering is followed in display and discussion of succeeding cross sections. At site 1909 Holocene deposits are the only Quaternary sediments present. The deeper units are channel fill, mostly clays, and were cored easily with two or three hammer blows [*Dames and Moore*, 1974]. The upper units are primarily sand or silty sand and, except for a stiff interval near 2-m depth, resisted coring only moderately more than the clays.

In the seismogram sections of profile 1909 (Figure 13) the

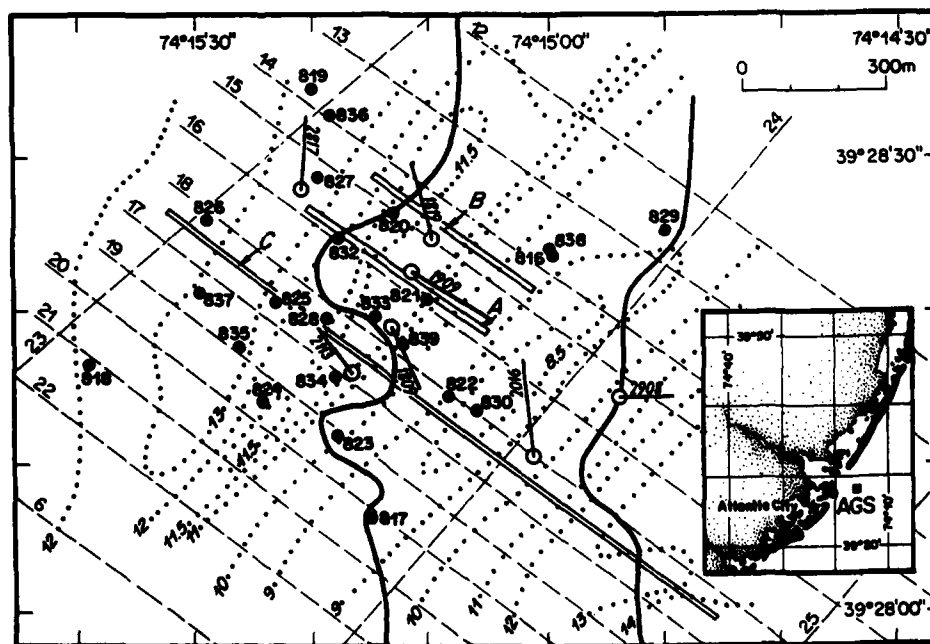


Fig. 11. Map of the Atlantic Generating Station (AGS) drilling site with inset to locate the area geographically. Dotted contours show bathymetry in meters, outlining a NE-SW trending sand ridge. Dashed lines 6 and 12-25 define a 1987 WHOI seismic reflection survey. Solid circles are boring locations, and open circles show source locations of shear wave profiles. The doubled lines A, B, and C locate cross sections shown in Figures 12, 15, and 16, respectively. The heavy sinuous lines show the approximate edges of a buried erosional channel defined by seismic surveys and core samples [*Dames and Moore*, 1974; *Miller and Dill*, 1974; *Stahl et al.*, 1974].

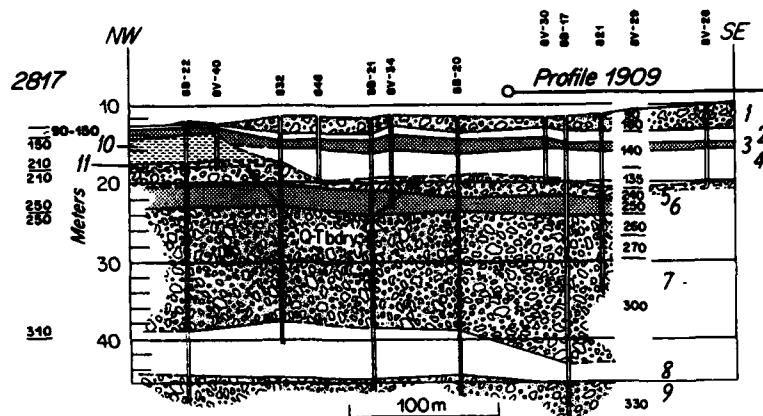


Fig. 12. Geologic cross section A modified from *Dames and Moore* [1974]. Coring locations are shown, some of which are located in the map of Figure 11. Shear wave velocities (in meters per second) versus depth are shown for profiles 1909 and 2817. The 1909 results are derived from waveform modeling, those for 2817 from ray tracing. Note that the channel with the landward edge near boring 832 eroded into the Tertiary beds and later filled with Holocene sediments. Note also the low velocity in strata 2–4 of the channel fill relative to strata at comparable subsurface depths outside the channel in profile 2817. The legend gives the major characteristics of the various strata and pertains also to cross sections B and C: 1, gray, medium-to-fine sand, trace silt, some shell fragments; 2, dark gray, silty clay, trace shell fragments occasional pockets/lenses of silty sand; 3, dark gray, medium-to-fine sand, some silt, occasional shell fragments, occasional laminations of silty clay; 4, dark gray, plastic clay, trace of fibrous organic material, occasional pockets/lenses of clayey sand; 5, light gray, medium/fine sand, trace silt, occasional gravel; 6, gray-white, fine sand, little to some silt, occasional stiff clay; 7, gray-white, medium/fine sand, traces of coarse sand, occasionally silty or gravelly; 8, gray-brown, very stiff silty clay; 9, essentially same as 7; 10, Pleistocene dark gray-brown, stiff fissured clay with lenses of silt, silty clay, and sand; 11, Pleistocene gray-brown, coarse-to-fine sand and medium-to-fine gravel.

low-velocity boundary wave is primarily influenced by the velocity structure in the Quaternary sediments and the earlier, higher-velocity phase is primarily influenced by the deeper sands below the Quaternary/Tertiary contact. The velocity model in Figure 14 (heavy line) and Table 1 represents our best fit to the data with full-waveform synthetics. Figure 14 also shows the velocity model for profile 2113, to be discussed later. The velocity values from the 1909 model shown in the geologic cross section (Figure 12) demonstrate the correlation between the lithology and shear wave velocity structure. The seismic data thus indicate a velocity range of 130–140 m/s in the deeper channel fill (below the 90 m/s seafloor sediment and higher-velocity lid) and velocities between 250 and 350 m/s in the Tertiary section.

The match of the synthetic seismograms with the recorded data is overall quite good. The Stoneley/Scholte waves are particularly well matched in both R and V components, clearly showing inverse dispersion. Amplitudes of the SV phases in R and V are noticeably different, but both are well modelled in the synthetics. A reasonable match for the SH phase in data and synthetics is obtained, but the later arriving Love wave is less well matched. The synthetics show higher frequencies (near 15 Hz) late in the wave train that are barely present in the data, which may indicate that the receiver toboggan was not well coupled to the seafloor at the higher frequencies, that the spectrum of the theoretical source function is too rich in high frequencies, or that Q at that frequency is lower in the upper sediments than the value used in the synthetics. The second layer in the seabed with velocity 180 m/s has only a slight, but favorable, effect on matching details of the boundary waves, and its velocity could be lowered to 140 m/s, as will be discussed later in the section on precision, resolution, and uniqueness. Note the

distinct high-velocity phase early in the T component synthetics, also visible in R, which is an artifact due to the 500 m/s cutoff phase velocity used in the calculations. This artifact is also present in other synthetic record sections, usually with lower amplitude. Inasmuch as the 1909 model has a basal layer with a velocity of 450 m/s, one might be inclined to associate the artifact with this layer velocity, unfortunately assigned a value near the cutoff velocity. However, we recomputed by replacing the 500 m/s cutoff velocity with 1000 m/s, which did not change the synthetics appreciably except for the artifact.

Profile 1809 also was recorded in the buried channel 120 m south of 1909 (Figure 11). These data are well matched to the full waveform synthetic seismograms for the 1909 velocity model, and are not shown. The geologic section also is similar to that near profile 1909.

The velocity data from profile 2817 are not as well constrained as in 1909 because adverse wind and current problems caused a nonlinear layout pattern and poor source and receiver alignments during the recording of the profile. The velocity-depth profile shown in Figure 12 was therefore produced by a ray trace inversion of the V component data. The results give velocities comparable to those of profile 1909 in the Tertiary sediments, with significantly higher average velocity in the Quaternary section. Along with other measurements, these data indicate a relatively uniform velocity structure for the Tertiary strata in the entire AGS area, which is not surprising in view of the significant lateral extent of these strata and of comparable core penetration rates at the various borehole locations. Thus most of the important variations in velocity structure are associated with the erosional and depositional processes active during the Quaternary.

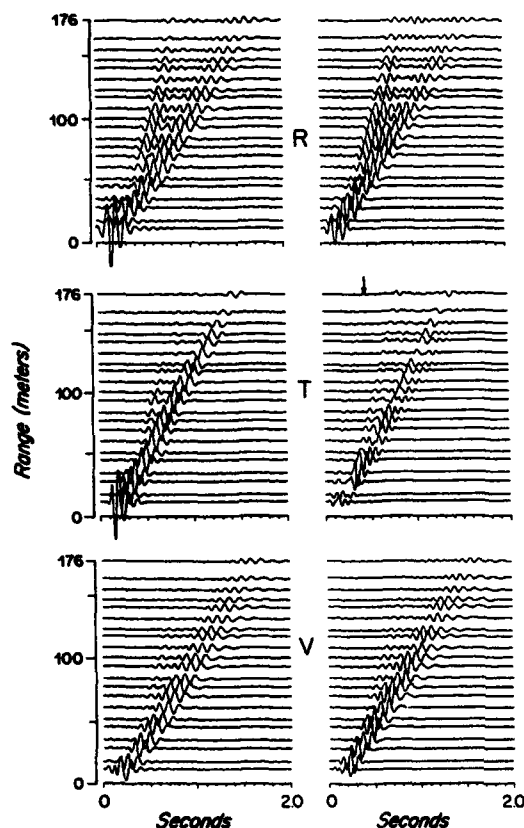


Fig. 13. Data (left) and synthetics (right) for profile 1909. Note inverse dispersion of the Stoneley/Scholte boundary wave in the R and V data and synthetics. Figure organization and amplitude scaling are the same as in Figure 8. The arrow in the T component points to a modeling artifact produced by a high phase velocity cutoff (500 m/s) in the synthetics, most prominent in T and R.

Cross Section B

The generalized subsurface structure along a transect from the flank of the sand ridge to the swale area northwest of the ridge is shown in Figure 15. The section is based on seismic reflection lines 14 and 15 and on borehole 820 data (Figure 11). Profile 1819 was recorded near this section; differenced T component seismograms are shown underneath. The profile crosses the western edge of the buried channel near borehole 820; the source location (fixed) is within the channel. The toboggan receiver sled was deployed on the west bank and, during the recording of the profile, was pulled across the channel edge. Thus the near trace data record the channel structure and produce seismograms similar to those of profile 1909. The main effects of the channel edge crossing are seen in the Love waves, which show a marked change of pattern between the near trace and far trace data. Note that the early, higher-velocity *SH* phase propagating in the Tertiary sediments is only mildly affected by the channel edge structure. However, a small increase in the *SH* amplitudes in the far traces could indicate a higher *Q* in the Pleistocene layers than in the Holocene layers.

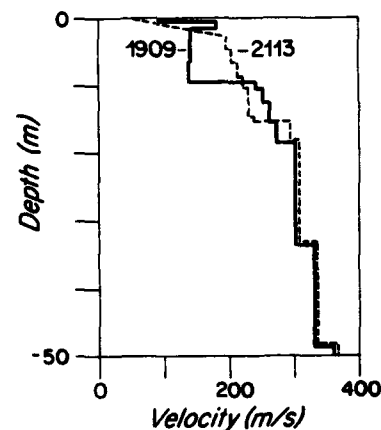


Fig. 14. Shear wave velocity model for profile 1909 (heavy line). This model also fits the data of profile 1809 and the short-range data of profile 1819. The light dashed line is the velocity model for profile 2113, shown later. The upper gradient layer is actually a series of six isovelocity layers in the model.

Cross Section C

Figure 16 serves both to show the geologic structure across the entire channel area and to provide a framework for discussion of profiles 2113 and 2016. The cross section is based on the data from the boreholes and on seismic reflection profiles, particularly lines 17 and 18 (Figure 11). Note that profile 2113 is located to the west of the channel. Shear wave data and synthetics for this profile are shown in Figure 17. These seismograms and the associated velocity model (Figure 14 and Table 1) are clearly different from those of profiles 1909 and 1819 previously discussed. The velocity-depth functions for the thick Tertiary sand (stratum 7) are similar in all the profiles, however. A major difference in the boundary waves is the inverse dispersion in 1909 and the long duration of normal dispersion in 2113 (compare

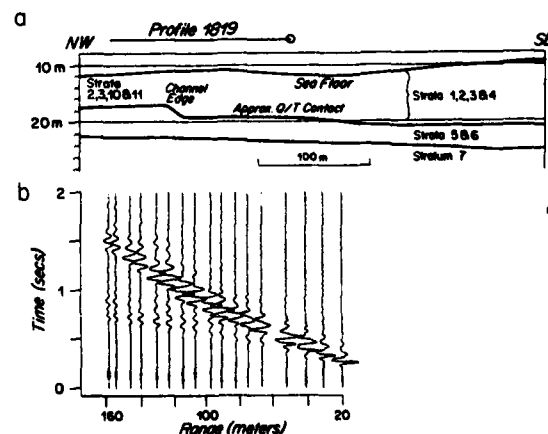


Fig. 15. (a) Geologic cross section B based primarily on the reflection data of lines 14 and 15, and compatible with borings 820 and 838. Note (in Figure 11) that seismic profile 1819 crosses the landward edge of the erosional channel. (b) T component data shown underneath the section display a significant disruption of the boundary wave at the point of crossing. A similar disruption occurs in the R and V component data. Strata identification as in Figure 12.

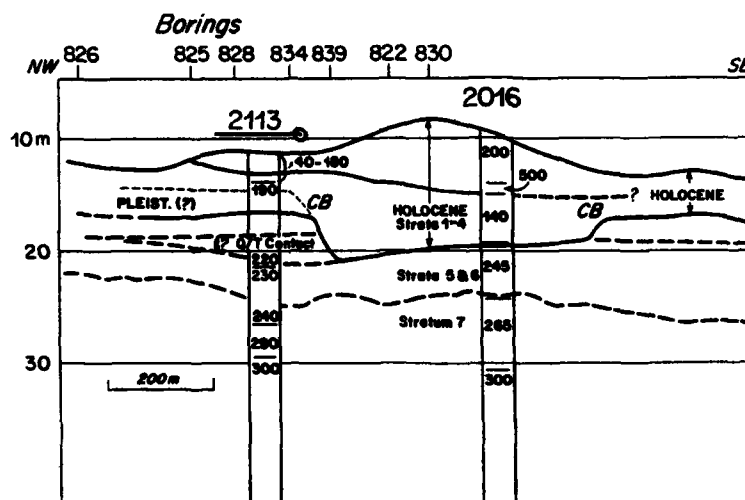


Fig. 16. Geologic section C crossing the sand ridge and underlying erosional channel, based on coring and reflection data. Also shown are seismic results from profile 2113, which is definitely outside the main erosional channel and from 2016 near the crest of the sand ridge. The dashed line at 14 m in the velocity column coincides approximately with the depth of sediments of early Holocene-late Pleistocene age, as determined by C_{14} analysis [Stahl et al., 1974]. Channel boundaries are denoted by CB.

Figures 13 and 17). Further, the clear separation of body and boundary waves in 1909, particularly in the horizontal components, is not observed in 2113. In profile 2113 the velocity is low (40 m/s) at the seafloor, increases rapidly to 190 m/s slightly above 3-m depth (possibly the Holocene-Pleistocene contact), then follows a much lower gradient through the Pleistocene and upper Tertiary. The most significant velocity discontinuity is at about 15 m. The two smooth positive gradient zones above 15 m are probably largely responsible for producing the long-duration boundary waves in this profile. The wave field in 1909, on the other hand, is greatly influenced by the thick, almost isovelocity zone between 1 and 10 m (Holocene channel fill) and the significant velocity discontinuity at the base of this layer.

The differences between the velocity functions determined for profiles 1909 and 2113 in the upper 10–15 m of the seabed as shown in Figure 14 are qualitatively confirmed by blow count data (Figure 18). These data points have been produced by the commonly used empirical relationship of Ohsaki and Iwasaki [1973], $G = 11.9N^{0.8}$, where G is the elastic shear modulus (in megapascals) and N is blow count, the number of blows of a 140-pound hammer falling 2.5 feet required to advance the core tube one foot into the sediments. Shear velocity values in Figure 18 are estimated by the equation $V_s^2 = G/\rho$ using a single value for ρ (bulk density) of 2050 kg/m³. The scatter in the blow count data would, of course, be somewhat reduced by using density values more appropriate to the specific layers and their depths, but a significant scatter would still remain. For example, had we used $\rho = 1700$ instead of 2050 kg/m³ in the low-velocity region above 10-m depth in profile 1909, the estimated velocities would have increased only 10–15 m/s. At greater depths, e.g., 20 m in profile 2113, substituting 2300 for 2050 kg/m³ would decrease the estimated velocity by ~30 m/s. Thus the overall scatter in velocities determined from the blow counts may be produced by the coring operation rather than by rigidity

variations. We have found that the blow count data are useful in a qualitative sense and that results are closer to the seismic data in the softer, finer grained sediment than in coarser materials. The presence of shell fragments or gravels in the latter could well account for non-uniform coring rates, and our seismic data at the greater depths seem to agree reasonably well with the lowest blow count values.

Figure 18 is useful also to compare the seismic and borehole results with data acquired in a contrasting geologic province and with data obtained with a different technique. The velocity versus depth profile in the panel on the right gives results from a vertical seismic profile using an SH, horizontal hammer, source and downhole sensors [Lash, 1980]. The measurements were made in the coastal plain south of Houston, Texas, approximately 20 km from the coastline. Below 3–4 m the sediments are water saturated and velocities can reasonably be compared with offshore results. Note that Lash's shear velocity profile has values significantly below those measured at 2113, a result consistent with typically high percentages of fine-grained components in the shallow sedimentary section of the Gulf coastal plain [Morton, 1988] as compared with the middle Atlantic region. Also shown in Figure 18 are results from a bottom shear modulus profiler (BSMP) measurement [Trevor and Yamamoto, 1991] close to our seismic profile 2113 in the AGS area. The BSMP method, introduced by Yamamoto and Torii [1986], is based on measuring the displacement of the seafloor by pressure variations caused by passing ocean waves. The response to this forcing function is measured by broadband seismometers buried just below the seafloor and the data are inverted for shear modulus versus depth in the seabed [Trevor et al., 1988; Yamamoto et al., 1989]. Although the BSMP does not resolve the high gradient in the uppermost sediment, it is encouraging that similar results are produced by such dissimilar techniques.

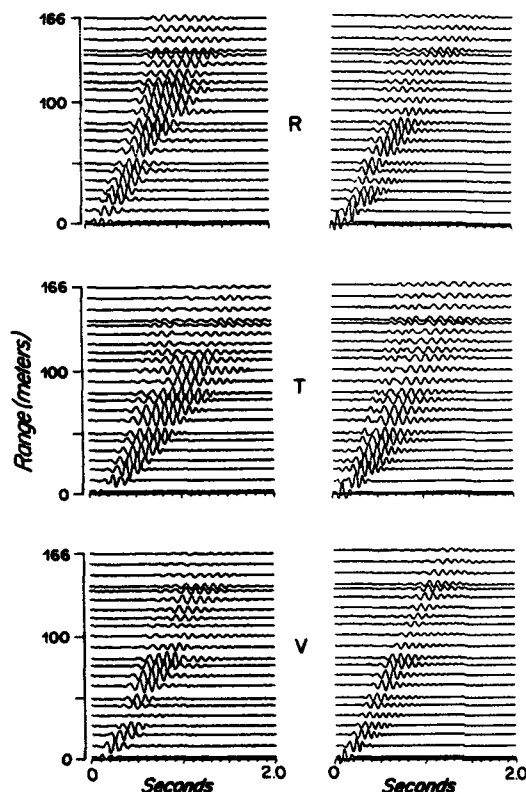


Fig. 17. Data (left) and synthetics (right) for profile 2113. Figure organization and amplitude scaling are the same as in Figures 8 and 13 except that in this figure the R and V amplitude scales are identical. Note normal dispersion and long duration of the boundary waves, which have lower group velocity in the T component than in the R and V components. The velocity model derived from these data is shown in Figure 14 for comparison with the 1909 model. These two models are shown again in Figure 18 for further comparisons.

Sand Ridge Profiles

Profile 2016 was recorded near the crest of the sand ridge (location in Figure 11). We show only the data and synthetics from the R and V components (Figure 19). The experiment layout was complicated by shifting wind and current, probably degrading the T, and possibly the R, data. The 2016 R and V seismogram sections differ significantly from those of profiles 1909, 1809, and 1819 recorded on the NW flank of the ridge where the upper sand is much thinner than that on the crest. In both locations, a few meters of soft Holocene clays lie between the sands of the ridge and the underlying Tertiary strata. Major differences in the seismograms are as follows: (1) phase velocities of the early arrivals are much higher in 2016 than in 1909, (2) the first shear energy arrives 100–150 ms earlier in 2016 than in 1909 at comparable ranges, and (3) the 2016 boundary wave phase velocities are higher (170 m/s in 2016 versus 130 m/s in 1909). Note that in both profiles, phase and group velocities are approximately equal. The boundary wave is poorly developed in 2016 and the record section is irregular, both in data and synthetics, especially in the R component.

Modeling of the 2016 data has been neither exhaustive nor wholly successful, although the general waveform and am-

plitude patterns are not seriously different from the recorded data at the shorter ranges. However, the synthetic boundary waves have higher amplitudes than the data, and the converse is true for the early, high-velocity arrivals. This may indicate the need for adjustment of the Q values. The most significant feature of the model that produced a reasonable match, listed in Table 1, was the insertion of a thin (1-m) layer with a velocity of 500 m/s at 5 m depth below the seafloor (approximate base of the sand ridge). Although such a layer seemed initially to be somewhat outrageous geologically, the blow count data at boreholes 817, 822, 829, and 830 indicated zones of difficult penetration at various depths in the sand ridge, at least somewhat in agreement with the seismic data. Further, models lacking the shallow, high-velocity layer produce synthetics greatly dissimilar to the recorded data. The only explanation we can offer for such high rigidity (4×10^8 Pa) at such a small depth in the seabed is to call on diagenetic processes in some way associated with migrating sand ridges in shallow water. (We thank our colleague and reviewer, D. G. Aubrey, for suggesting that the high velocity might have been formed initially as a "pavement" in the sand wave trough and that the ridge has migrated over it subsequently.) The reliability of the results from this profile is discussed further in the section on precision, resolution, and uniqueness.

Profile 2908 (location in Figure 11) was recorded on the southeast flank of the sand ridge, where the thickness of sand is intermediate between that of profiles 2016 and 1909. In this profile (not shown) the overall pattern of the data is similar to that of 2016 but with lower phase velocities of the early arrivals. Further, the boundary wave is even more

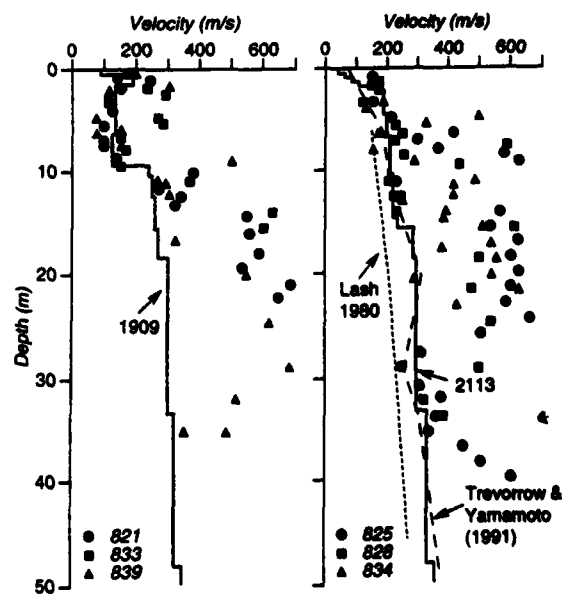


Fig. 18. Comparisons of shear velocity versus depth profiles determined by seismic measurements and by inversion of blow count data [Ohsaki and Iwasaki, 1973]. The method is discussed in the text. Three borings closest to profiles 1909 and 2113 provided the blow count data. Comparison is also made between these profiles and a vertical seismic profile in the Gulf Coast south of Houston, Texas [Lash, 1980]. The Gulf Coast velocities are lower, but the velocity gradients are similar. Data from a BSMP measurement [Trevorrow and Yamamoto, 1991] are also shown for comparison.

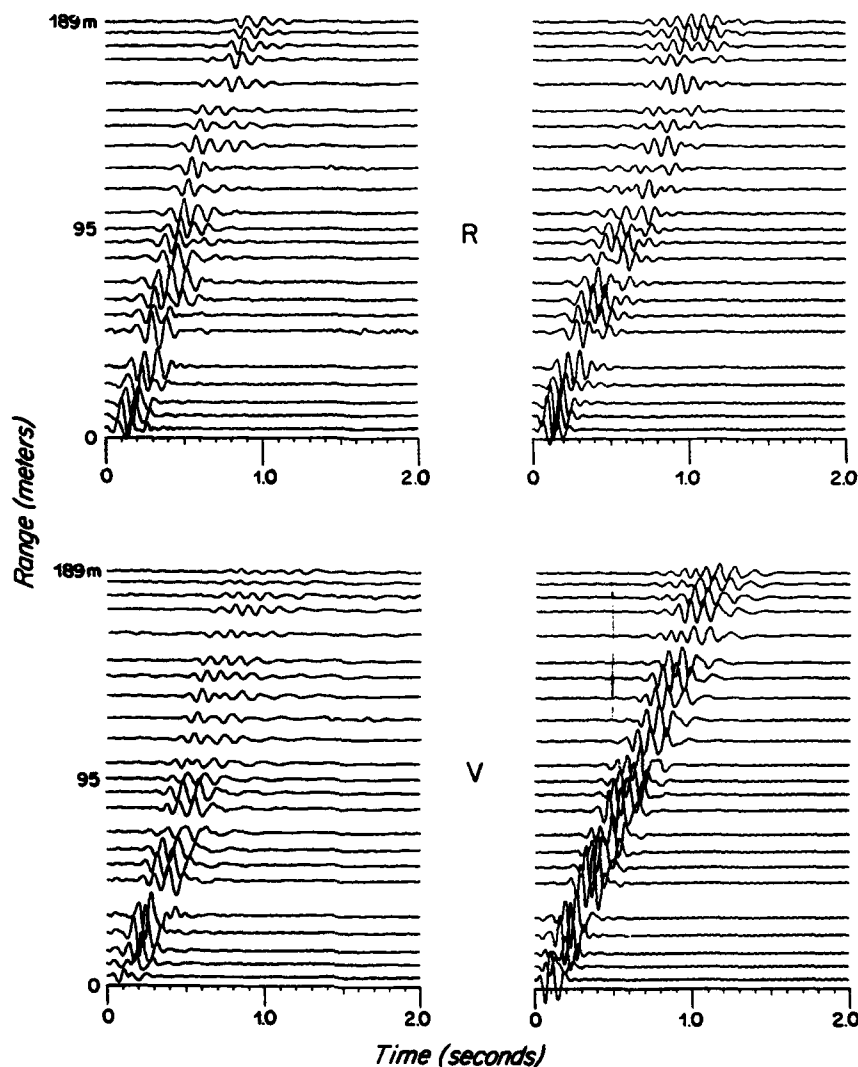


Fig. 19. Data (left) and synthetics (right) seismograms of the R and V components of profile 2016 recorded near the crest of the sand ridge (Figure 11). Details of the data and waveform modeling are discussed in the text.

poorly developed, which is not surprising inasmuch as this profile was recorded with the source located on or near the eastern edge of the buried channel and the line of receiver locations extended onto the eastern bank.

AMCOR 6009

This drill site is on the outer continental shelf in approximately 60-m water depth (Figure 1). Hathaway *et al.* [1976] and Richards [1977] report the upper 68 m of seabed to consist of 5 m of silty, sandy clay overlying 10 m of sand and 53 m of silty, sandy clay. Figure 20 shows a line drawing of a Hunttec high-resolution reflection profile through the site, in which the top and base of the sand layer correlate well with reflections approximately 6 ms and 18 ms below the seafloor. A reflecting surface at 9–10 ms (within the sand layer) has no correlation with the coring results. Note that the sand layer apparently extends horizontally beneath the rise in the seafloor on the left side of the diagram. Three

shear wave data sets were acquired near the drill site during the two cruises. Their locations and the drill site are projected onto the reflection profile.

Profile 6009G was recorded with the 1988 geophone array and a shotgun sled source with inclined cannons (Figure 2b) and 200-grain loads. In profile 6009L the ladder array was used, with the same source sled, but with eight-grain loads. Profile 2715 was recorded with the toboggan receiver package and an air gun source, suspended near the bottom. The two array measurements provided only shallow velocity information, but at high resolution, whereas the air gun-toboggan profile measured velocities at greater depth but with poorer shallow resolution.

T component data of profile 6009G and matching synthetics are shown in Figure 21. The principal result is a well-developed Love wave that is matched by synthetics computed for a model with a layer 1.12 m thick with $V_s = 86$ m/s over a 209 m/s half-space (Table 1). The model used for the

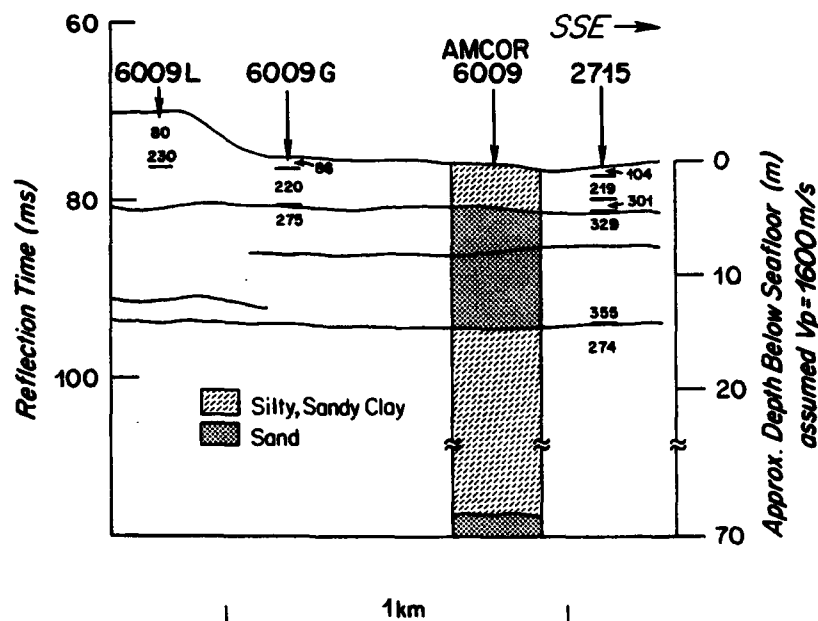


Fig. 20. Line drawing of Huntex high-resolution reflection data near AMCOR 6009. Shear velocity sections from three measurements in this area are projected onto the reflection section, along with core data of Hathaway *et al.* [1976].

synthetics was obtained by matching the phase and group velocities and the frequency of the data to the theoretical Airy phase for Love waves for a single layer over a half-space. Assuming a reasonable density ratio provides a unique solution for the two shear velocities and the layer thickness. The amplitude falloff with range establishes a Q estimate of 40 in the layer and in the half-space. The data seismograms are noisy between the water waves and the Love wave, but some weak SH arrivals from the half-space are visible. However, the signal/noise ratio is too low to permit resolution of the half-space velocity structure. The match of the Love wave by the synthetics is good, clearly defining the presence, and a precise estimate of the velocity and thickness, of the thin upper layer. In the R component of profile 6009G (not shown) there is only one phase velocity (220 m/s) clearly observed and a second poorly constrained velocity of 275 m/s. These velocities were used in a two-layer delay time calculation, the results of which are shown in Figure 20, and indicate good correlation of the 275 m/s velocity with the upper boundary of the sand layer about 4 m below the seafloor. The uppermost velocity, 86 m/s, is based both on estimates of direct travel times from the source to radial geophones at 2 and 4 m range and the analysis of Love wave data discussed earlier. Thus the velocity structure of profile 6009G is a composite of T and R data.

The second profile in this area, 6009L, was located on a topographic high NW of the drill site and recorded with the ladder array (see Figure 20 for location). Figure 22a shows V component seismograms with expanded time scale, and Figure 22b shows the same shot recorded by the T component, with less time scale expansion. The source was an inclined-barrel shotgun cannon with an eight-grain load. Note that the dominant frequency recorded by the vertical component is 40–50 Hz, whereas frequencies between 25 and 80 Hz are present in the transverse component. These are, single shots, neither summed nor differenced. The V

data show clearly the presence of a high-velocity gradient in the uppermost sediments. The same gradient is recorded in the T data which also shows the velocity increasing to a value of ~ 230 m/s at the maximum range of the profile. By use of well-known ray theory equations for calculating velocity gradients and penetration depths [Nettleton, 1940] and assuming linear gradients, we estimate the upper 4–5 meters of sediment to have a gradient of $25\text{--}30\text{ s}^{-1}$, as shown

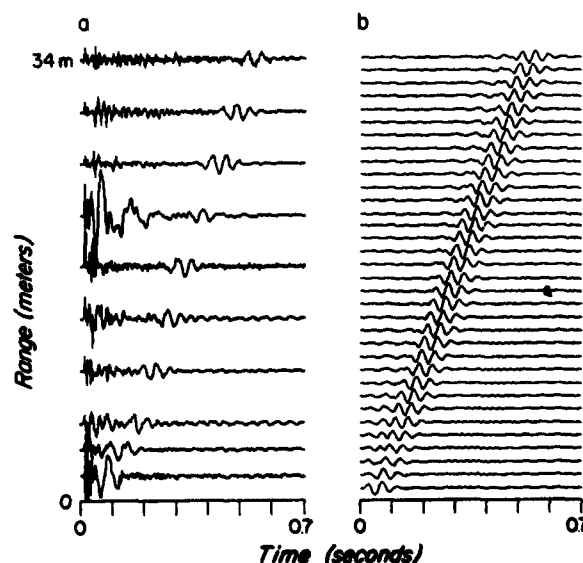


Fig. 21. (a) T component geophone data and (b) synthetic seismograms for profile 6009G. A simple model for the synthetics (Table 1) consists of a 1.12-m-thick layer with a velocity of 86 m/s over a 209 m/s half-space. Matching of the Love wave data was the primary goal for this data set.

in Figure 20. The normal dispersion in the T component also is indicative of velocity increase versus depth, although we have not modeled it. This data set demonstrates the value of close spatial sampling to determine velocity structure of the shallow seabed.

The deeper velocity structure in the area has been estimated by matching the 2715 data and full waveform synthetics with emphasis on source-to-sensor ranges beyond 30 m. The V component seismograms and synthetics are shown in Figures 23a and 23b, respectively, and the model parameters are listed in Table 1. The R and T components did not provide useful data. The overall match is satisfactory for travel times, phase velocities, and amplitude distribution. However, the frequencies are lower in the synthetics. This discrepancy suggests that some combination of shear velocity, thickness, and Q used in the shallow layers for the synthetics could be improved. The earliest, high-velocity phase in the synthetics is produced by the 500 m/s high phase velocity cutoff, and its interference appears to distort the legitimate first arrivals and probably helps to create travel time discrepancies between data and synthetics. The maximum wavelengths in profile 2715 are approximately 30 m and should be sensitive to velocity structure to a depth of at least 15 m, which is near the base of the sand layer. In the model used to compute the synthetics, we have assumed a velocity inversion at this depth, corresponding to the transition from sand to the underlying silty, sandy clay. *Trevorrow and Yamamoto* [1991] deduced a velocity inversion at 10-m depth from a BSMP measurement in the vicinity of 6009 which supports the assignment of a relatively low velocity in

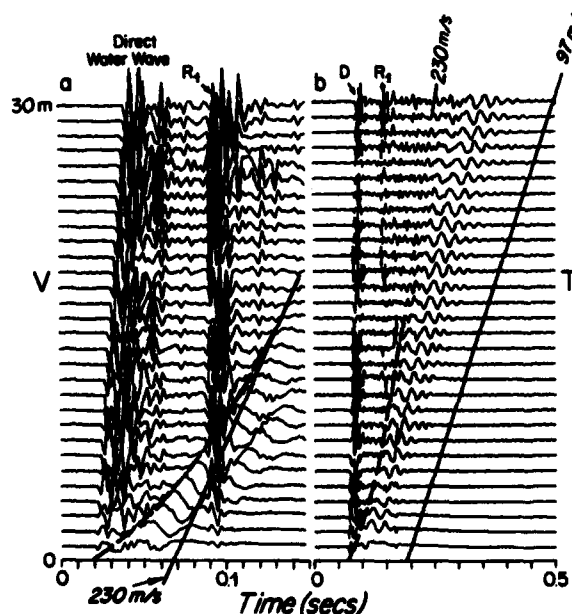


Fig. 22. (a) Vertical and (b) transverse component data, respectively, recorded with the ladder array at profile 6009L (Figure 20). The strongly curved arrivals, highlighted by dashed lines, indicate velocity increasing from approximately 80 to 230 m/s. The T component (Figure 22b) clearly shows the higher phase velocity in the far traces. Note the normally dispersed Love waves, also indicative of increasing velocity with depth. The 97 m/s reference line in (Figure 22b) approximates the seafloor velocity. There is a time delay in the array data; zero time corresponds to the intersection of the direct water wave with the time axis.

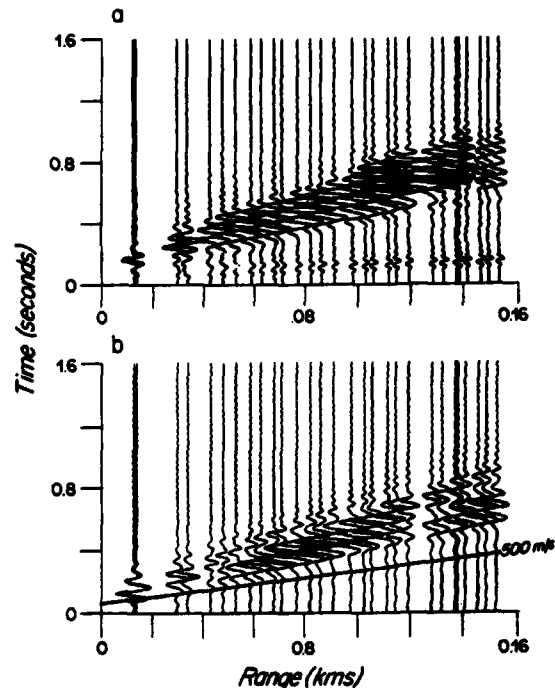


Fig. 23. (a) V component data and (b) synthetic seismograms for profile 2715. Reference line in (Figure 23b) is drawn on an artifact produced by the high phase velocity cutoff (500 m/s). The earliest arriving seismic data have phase velocities between 300 and 355 m/s (Table 1).

our model below 14-m depth. An interference pattern developed in the far traces of the 2715 seismogram section might be interpreted as an effect of either a velocity inversion or a horizontal discontinuity. Hence we consider that this interpretation of the profile probably provides uncertain information about the geology deeper than 14 m and, unfortunately, does not offer a satisfactory comparison with the BSMP results.

AMCOR 6010

Although we recorded no shear data at the 6010 site, useful results were obtained at a location approximately 5 km toward the northwest (site 6010 NW in Figure 1). Some discussion of the regional geology may help to put these results and those of site 6009 into perspective.

High-resolution reflection profiling of this area [Milliman *et al.*, 1990; Davies *et al.*, 1992] during the past few years has indicated an important lateral boundary in the shallow sedimentary section that lies between sites 6010 and 6010 NW. The boundary has been best mapped in the region around these two sites (Figure 1). Milliman *et al.* [1990], suggest that seaward of the boundary a broad wedge of post-Wisconsinan sediment has been deposited on the outer shelf and slope on an erosional surface developed during the low sea level of the last glacial maximum. Landward of the boundary the erosional surface crops out and constitutes the seafloor. At site 6010 these recent sediments are approximately 20 m thick; at site 6009 they are locally variable in thickness (≤ 5 m) and, in fact, may be present only in small pockets.

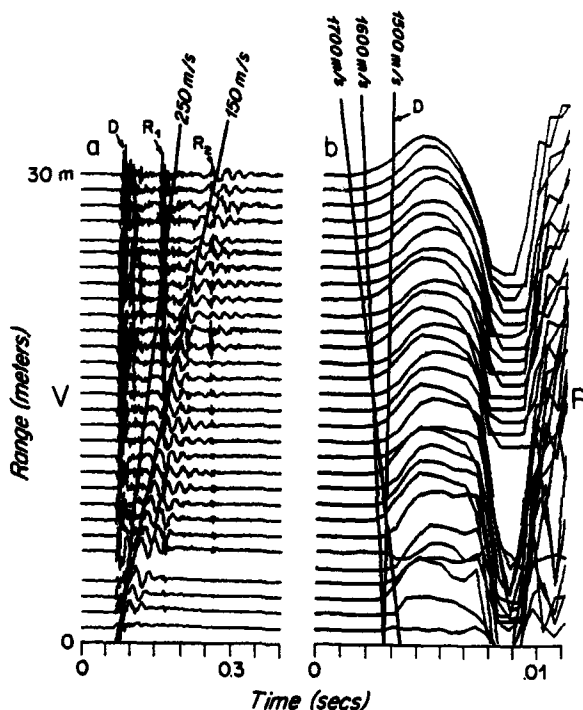


Fig. 24. V and P component ladder data from site 6010 NW. Real zero time is at (a) 70 ms and (b) <3 ms. Small intercept times of the reference lines indicate relatively high velocities for both S and P at very shallow seabed depth.

As noted earlier, the shear velocity at the seafloor near AMCOR site 6009L is 80 m/s, with a rapid increase to 230 m/s at 5-m depth in the seabed. The time intercept for 230 m/s in this profile is ~48 ms. The profile at 6010 NW (Figure 24a) gives a contrasting result, with both the highest shear phase velocity of 250 m/s and the slower boundary wave velocity of 150 m/s having essentially zero time intercept. These results are thus consistent with a thin layer of post-Wisconsinan sediment at 6009, which is absent at 6010 NW. Although we did not record shear wave data at site 6010, P wave refraction profiles approximately 300 m long were recorded near both 6010 NW and 6010 as an auxiliary experiment during a 1989 reflection cruise by J. Ewing and J. Austin. These measurements were made by deploying a hydrophone on the seafloor and recording the Huntco boomer source, which was towed approximately 20 m above bottom. The recorded frequency bandwidth was 1–3 kHz, and profile lengths were 200–300 m. Hydrophone cable was payed out during recording and recovered after each profile. At 6010 NW a P wave refraction is observed with a velocity <1700 m/s and an intercept time of 1–2 ms, which is consistent with P data recorded in the same area by the ladder array (Figure 24b). In contrast, the data at comparable or greater source-receiver ranges at 6010 gave no indication of refracted energy arriving ahead of the water wave, which indicates either a low P velocity (<1500 m/s) or absence of a positive velocity gradient in the upper sediments. We expected to record refracted arrivals from the buried erosional surface at ~20-m depth, but apparently the boomer sound source was not powerful enough to overcome the attenuation. A shear wave (P/SV) profile at site 6010

[Stoll et al., 1991] shows a nondispersive boundary wave with a velocity of ~200 m/s and an SV refraction with a velocity of ~350 m/s intercepting the time axis at 160 ms. A slope/intercept calculation with these parameters gives a depth of 20 m to the high-velocity layer in excellent agreement with the reflection data.

Site South of Martha's Vineyard (MV)

Site MV (location in Figure 1) is in the northwestern fringe of the well-known "Mud Patch" [Bothner et al., 1979; Twichell et al., 1981], a large area (13,000 km²) of the middle/outer continental shelf south of Martha's Vineyard covered by anomalously fine-grained recent sediments. The thickness of these deposits ranges between 10–12 m maximum and zero on the fringes. It is therefore not surprising that the measurements at this site show low shear velocity in a thin uppermost layer. Further evidence for a soft bottom was the finding of significant quantities of mud filling cavities in the hardware after the array had been recovered.

Results from modeling ladder array data are shown in Figures 25 and 26. T synthetics for four velocity-attenuation models are shown in Figure 25, and R and T data are compared with synthetics of model 4 in Figure 26. The rapid change in both phase and group velocities observed within the first few meters of range contains information about the uppermost sediments that could be lost or ambiguously interpreted from data with coarser sampling. In the models of Figure 25 we are mainly trying to match the later parts of the wave train of the T component data. Model 1 approximates a linear velocity gradient; model 2 has a more realistic gradient decreasing with depth; models 3 and 4 have a low-velocity layer, less than 1 m thick at the top. In all models, Q (amplitude attenuation is proportional to $\exp[-\pi f r / Q v]$, where f , r , and v are frequency, range, and velocity, respectively) is finite; only model 4 Q values are shown in Figure 25 (25 in the upper layer and 50 beneath it). The T component seismogram sections are shown underneath the models. All phase velocities less than 500 m/s are included in these synthetics. When comparing models 1 and 2, we see that the higher-velocity model 2 produces the lower prominent group velocities; the high near-surface gradient in model 2 traps much low-velocity energy. Compared to the data (discussed below), model 1 is too fast and model 2 is too slow. Models 3 and 4 provide better matches to the data; model 4 shows a better fit to the T data.

In Figures 26a and 26b, model 4 synthetics for R and T components are compared with the data. Both phase and group velocities match well, but the signal durations could be better matched. The R synthetics and the T data have the longer wavetrains. Figure 26c is a comparison between the model 4 T synthetics and the T data obtained during the same deployment but from a shot at the opposite end of the array. The wave trains are shorter, and the match with synthetics is excellent. The existence, thickness, and shear velocity of the low-velocity layer in model 4 are corroborated by treating the large-amplitude late arrivals on the reverse-transverse record section as being the Airy phase of the fundamental mode Love waves, as discussed for profile 6009G. Matching the frequency and the group and phase velocities of the data with the theory for a single layer over a uniform half-space, using a density ratio of 1.3, we obtain a thickness of 0.8 m and shear velocities of 37 and 105 m/s for

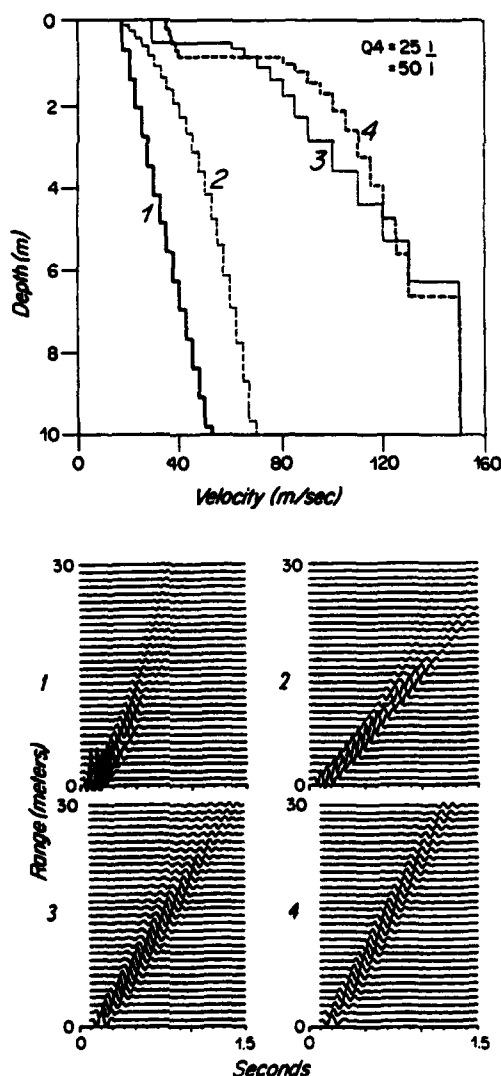


Fig. 25. Four velocity models (upper) and corresponding synthetic seismograms (lower) computed for the T component at site MV. In models 3 and 4, Q_4 values of 25 and 50 were used for the upper and lower gradient zones, respectively. Real zero time for 1 and 2 is 0; for 3 and 4 it is 70 ms.

the layer and half-space, respectively, in good agreement with model 4.

The differences in data character between the forward and reverse profiles may result from some movement of the array between shots or different source coupling to the bottom. Alternatively, they may also indicate a real variation in the seabed between the two ends of the array. Indeed, the forward-transverse data (Figure 26b) are better matched than the reverse-transverse data (Figure 26c) to the model 3 synthetics (Figure 25) and the converse is true for the model 4 synthetics. Inasmuch as these measurements were in the fringe of the Mud Patch, shots at opposite ends of the 30-m-long array could produce significantly different seismograms, particularly in the boundary wave.

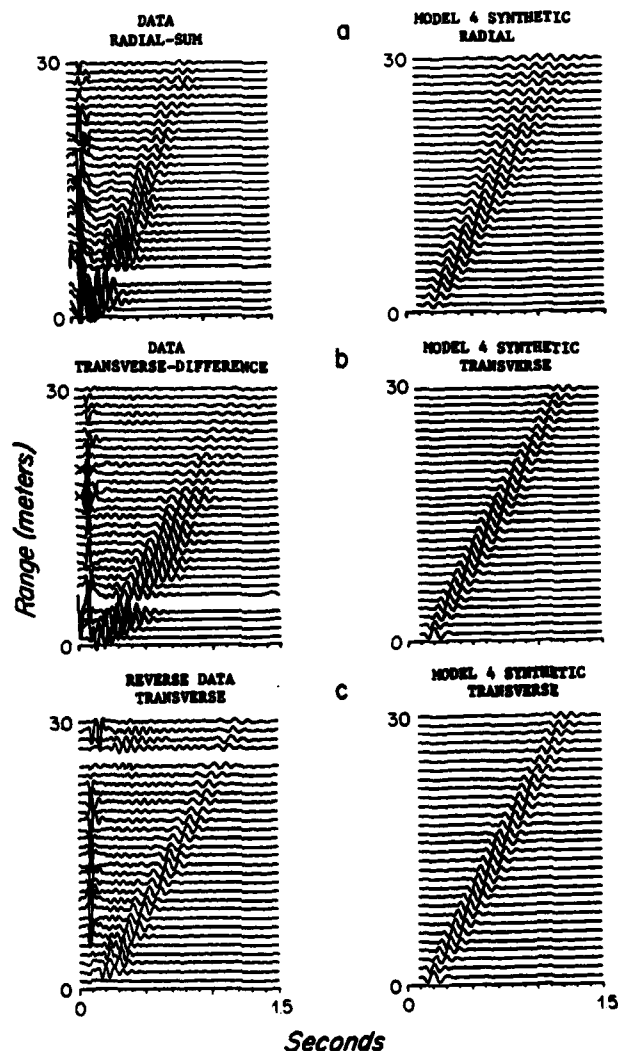


Fig. 26. Data and synthetics for model 4 (Figure 25) are compared for (a) R component and (b) T component. (c) Comparison of T data from a shot at the opposite end of the array with the same synthetics. See discussion in the text. Real zero time is 110 ms in all cases.

Hydrophone Data

In this paper we have emphasized the analysis and interpretation of the ground motion data, partially because of our emphasis on *SH* propagation. The ground motion data are more likely to be subject to distortion than the hydrophone data because of poor coupling to the bottom and the possible influences of differential horizontal motion across the water/sediment interface [Sutton and Duennebier, 1987]. Thus it might be expected that matching the motion data with synthetics would be more difficult than for the pressure data. However, pressure data, when combined with the motion data, can, for example, provide additional information on the direction of energy propagation and on subbottom impedances [White, 1965; Stickler, 1975]. Although we have not modeled the low-frequency *P* data, the overall wave field patterns are similar, and the relative amplitudes and phase relationships relative to *V* and *R* data are as expected.

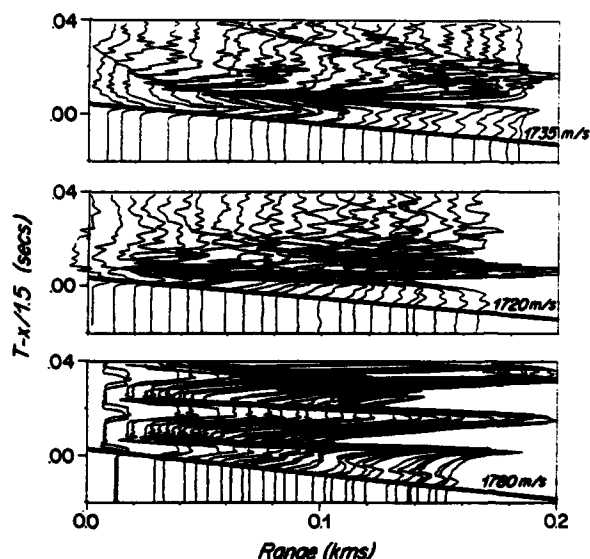


Fig. 27. Examples of *P* wave data recorded with the hydrophone during the 1986 cruise. Data were sampled at 1-ms intervals; amplitudes are scaled proportional to range. The profiles, top to bottom are 2509 (AMCOR 6011), 2113 (AGS) and 2715 (AMCOR 6009). Reference lines indicate *P* velocities at depths of 5–10 m.

Examples of high-frequency, unfiltered compressional wave data recorded at profiles 2509, 2113, and 2715 in the 1986 field program are shown in Figure 27 (an example of high-frequency *P* from the ladder array was shown in Figure 24b). Velocity reference lines correspond to *P* wave refractions between 1720 and 1780 m/s. The positive intercepts of these lines with the travel time axis indicate the presence of sediment with velocity lower than 1700 m/s occupying the upper 5–10 m of seabed, as estimated by the slope/intercept method and assuming a *P* velocity of 1600 m/s for the top layer. These thicknesses would be reduced by approximately 1 m if the upper layer velocity were 1550 m/s instead of 1600. Resolution of layer thicknesses in these data is not high because the wave lengths corresponding to the 60–80 Hz dominant energy are 20–25 m. Data from the ladder array give a fair measure of lower velocities in the uppermost seabed. In *P* component data at 6009L and at site MV, refracted energy is not discerned in the nearest 15–20 traces, indicating a low seafloor velocity. The outer traces show arrivals 1–1.5 ms ahead of the water wave indicating a velocity near 1600 m/s. The precision of these velocity measurements is limited by the 0.5-ms sampling rate and 30-m profile length but is sufficient to determine a seafloor velocity as low as 1540 m/s.

Of peripheral interest is the comparison of the wave forms in these unfiltered hydrophone data. The source for profile 2715, in the lower panel of Figure 27, was a standard airgun suspended near the seafloor. There is a significant bubble oscillation in the signature, which does not appear in the other profiles recorded with the airguns confined in the "cannon barrels". The confinement serves as an effective bubble pulse suppressor.

PRECISION, RESOLUTION, AND UNIQUENESS

No formal objective error bounds have been established for the velocity/attenuation models presented in the preced-

ing sections and questions of precision, resolution and uniqueness were addressed only tangentially. Preliminary attempts at direct numerical inversion of the record section data to produce phase velocity dispersion curves using the procedure of McMechan and Yedlin [1981] and to transform the data directly into velocity-depth sections using the method developed by Clayton and McMechan [1981] were not encouraging and not pursued further. However, it is possible that future attempts will be fruitful.

In this paper we have concentrated on estimating the shear velocity/attenuation structure by applying the methods of full-waveform forward modeling. Except when indicated in the preceding section, compressional wave velocities were assumed to vary from about 1600 to 1800 m/s as expected for shallow marine sediments. Poisson's ratios are 0.46 or greater and generally above 0.48. Densities also were estimated in a similar manner, varying from about 1500 to 2000 kg/m³. It is unlikely that errors in these estimates produce a significant error in the shear wave models. This assumption was tested using the model for profile 1909: compressional velocities were changed from a range of 1600–1750 m/s to a range of 2000–2050 m/s with no apparent change in synthetic seismograms; densities were changed from a range of 1700–1800 kg/m³ to a constant value of 2000 kg/m³, also with no apparent change in the synthetic seismograms.

As discussed in the section on seismic waveform modeling, preliminary velocity models generally were obtained using standard travel time techniques. These models were then refined by trial and error, matching synthetic seismograms to the data. In this latter procedure, expected velocity and frequency characteristics of reflected, refracted, and guided waves were used to indicate appropriate modifications to the models. Additionally, lithological data from boreholes provided information on possible velocity discontinuities and velocity inversions.

As might be expected, models requiring velocity inversions (or thin, high-velocity zones) were the most difficult to model and probably have the greatest remaining uncertainty. For example, the seismic evidence for the shallow, thin, high-velocity zone (180 m/s) in AGS profile 1909 is weak (Figures 13 and 14, Table 1) although the general match between data and synthetics is good. The thickness of the 180 m/s layer in the model is a small fraction of most of the wavelengths in the data.

In the model for AGS profile 2016, however, the high velocity layer (500 m/s) between 5 and 6 m subbottom and the low velocity zone beneath it are required to match the data (Figure 19, Table 1). In Figure 28 we compare the *R* and *V* synthetics for the 2016 model with those for a simplified model having a uniform 250 m/s half-space below the 500 m/s layer. The differences are striking. In contrast with the simple normal dispersion, predominantly boundary wave energy from above the 500 m/s layer in the simplified model, the synthetics for the actual model display a complex interference pattern, especially on the *R* component, between the shallow energy and that associated with the deeper structure. "Example" models with and without a low-velocity zone (LVZ) are compared in Figure 29 to illustrate some of these same effects. The model without the LVZ produces a regular pattern of refracted and boundary wave energy, whereas the LVZ model produces a more complex pattern, especially on the *R* component. Note also that while the boundary wave is inversely dispersed in both models, the

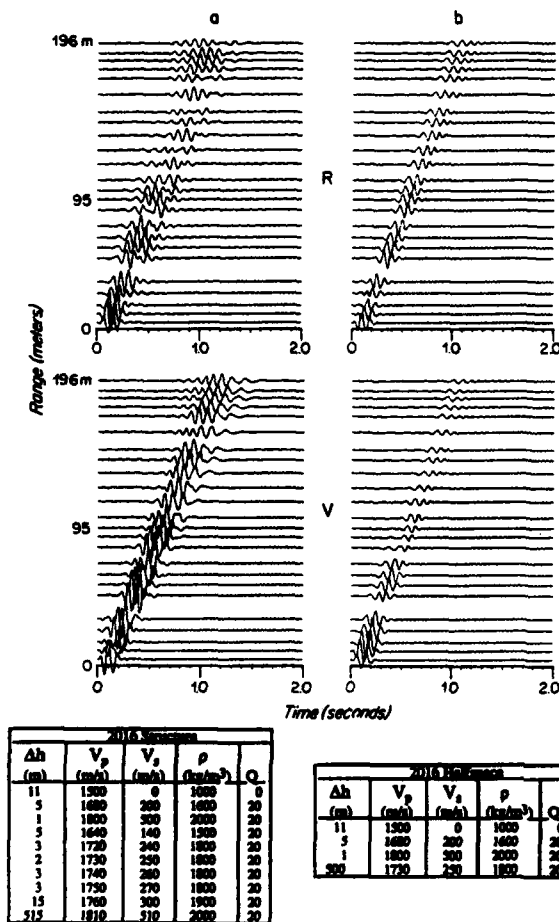


Fig. 28. Comparison of synthetics of (a) the final model for AGS 2016 with (b) in which the section below the thin 500 m/s layer at the base of the sand ridge is replaced by a 250 m/s half-space. Amplitude scales for R and V are equal in Figure 28a; in Figure 28b, V amplitudes are reduced relative to R by a factor of 2.3.

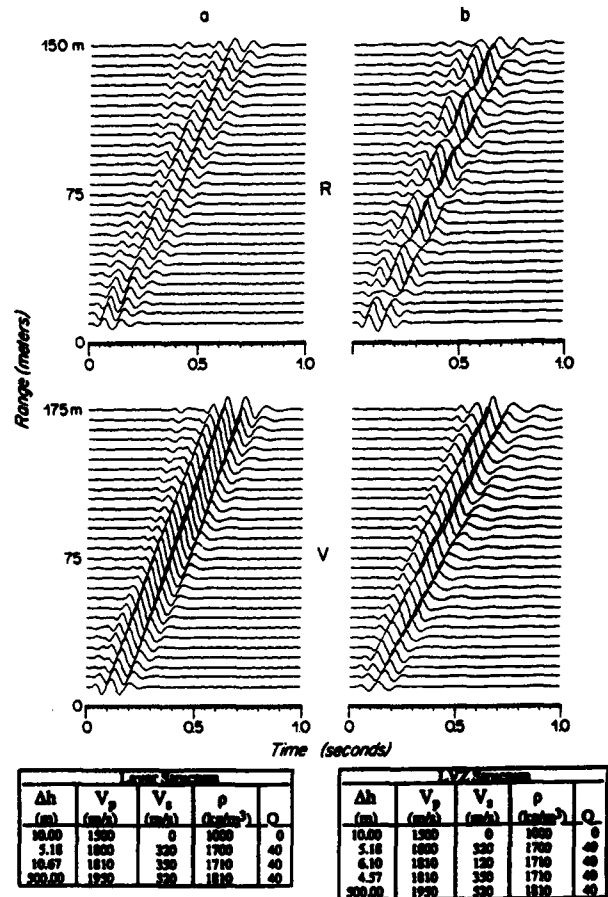


Fig. 29. Comparison of simple water-covered structure (a) without and (b) with a low velocity zone (LVZ). V amplitudes are reduced relative to R by 0.67 in Figure 29a and by 0.33 in Figure 29b, i.e., the V/R ratio is approximately 1.5 for Figure 29a and 3 for Figure 29b. Although both structures produce inverse dispersion in the frequency band displayed, phase velocity is higher than group velocity in Figure 29a and less than group velocity in Figure 29b.

phase velocity is higher than the group velocity in the model without the LVZ and lower than the group velocity in the LVZ model.

Generally, the velocities of the uppermost sediments are well determined. For example, small changes in the gradient and thickness of the high gradient zone in AGS profile 2113 (Figures 14 and 17 and Table 1) strongly affect the frequency and duration of the low group velocity energy. Differences between model and data frequencies at a given velocity were used to guide adjustment of depth/velocity ratios in the modelling.

In the model for profile 2016 (Figure 28 and Table 1) the lowest-order frequency for multiple, critical angle reflections in the sediments above the 500 m/s layer is about 11 Hz. This frequency is prominent in the synthetics in both the full model and the simplified model, especially at larger ranges. It is also present in the data, lending some support to the reliability of the model. However, since the maximum of the theoretical source spectrum is 10 Hz (Figure 5), we would expect large amplitudes near that frequency. The frequency, group velocity, and phase velocity of the pulselike Love wave in profile 6009G (Figure 21 and Table 1) and at the MV

site (Figures 25 and 26), when interpreted as the fundamental mode Airy phase for a single layer over a half-space, provided a strong constraint and check on the velocity and thickness of the low-velocity uppermost sediment as well as an estimate of the deeper velocities. The estimate of thickness appears to be good to a few centimeters (less than 5% error), and the layer shear velocity has an even smaller error. Note that the predominant frequency (24 Hz, used in the Love wave calculation) in the 6009G Love wave is near the maximum of the theoretical source spectrum (Figure 6) and augments its amplitude, but the 13 Hz used for the MV profile is roughly half the source maximum. It is interesting to note that the critical angle resonance conditions for the Love wave models are 21 and 12 Hz for 6009G and MV, respectively.

The precision and resolution of the derived velocity models can be estimated from comparisons among synthetics from similar models. Most of the models presented in this paper are the result of comparing the full waveforms from a number of related models with the recorded seismograms and picking the closest match. The 5% difference between

TABLE 2. The e^{-1} Corner Frequencies Versus Travel Time and Q

Q	Travel Time, s		
	0.25	1.0	1.5
10	12	3	2
20	24	6	4
40	52	13	9
80	100	25	17

Frequencies are in hertz.

the upper portions of the P/SV and SH models, indicating anisotropy at the AMCOR 6011 site (Figures 8 and 9 and Table 1), was clearly required by the data. The strong differences in the synthetic record sections from four models for the MV site shown in Figure 25 provide further evidence for the sensitivity to different models. In general, we believe the velocity models have an uncertainty of 10% or less in the upper portions of the derived sections and somewhat more for the deeper portions. Possible errors in derived low-velocity zones are expected to be larger, with possible trade-offs between velocity and thickness to produce similar delay times. For example, the depth to the bottom of the 140 m/s low-velocity layer in the model for profile 2016 (Figure 28, Table 1) was chosen to agree with borehole and seismic reflection profile results; changes of more than one meter, with appropriate change in velocity, would probably produce quite similar record sections. Some trade-offs between gradients and Q of deeper layers can also produce comparable record sections.

A finite Q , was always required in order to achieve a good match between data and synthetics. Q affects, among other things, the relative amplitudes between early and late arrivals, the amplitude fall off with range, and the maximum observed frequencies. In our modeling we found that frequency-independent shear wave Q of 20 or 40 in individual layers (25 and 50 in the MV synthetics) provided an adequate match. Compressional wave Q was arbitrarily set at 1000. A shear wave Q of 80 generally appears to be too large and Q of 10, too small. Of course, the effects of Q are extremely nonlinear. A useful guide to when Q becomes important is the e^{-1} point ($N = Q/\pi$, where N is the number of periods (f^{-1}) in the travel time when attenuation reduces the amplitude by e^{-1}). For example, $N = 3, 6, 13$, and 25 is equivalent to $Q = 10, 20, 40$, and 80 respectively. Table 2 gives e^{-1} corner frequencies for appropriate travel times and Q . The amplitude near the corner frequency drops abruptly for travel times greater than those listed in Table 2. Additionally, if Q is not frequency-dependent, at a given travel time the amplitude drops abruptly for frequencies above the corner frequency.

Predominant frequencies in our data lie mostly between about 10 and 50 Hz. However, in interpreting Table 2 we remember that the source time function, receiver frequency response, and bottom coupling, and the velocity structure also affect the spectra of the data. Comparison of synthetics and data for profile 2113 (Figure 17 and Table 1) with two different Q models suggests that the high-gradient upper zone might require a larger Q for SH than for SV (or that the velocity structure might be slightly different). The model shown has the lower Q and fits the SV data somewhat better.

The Q values used in generating the synthetics and listed in Table 1 were not given the same attention as the velocities in developing the models and are not as reliably related to the lithology. However, for example, the reduced values (20 and 25) in the upper portions of the 2113, 2715, and MV models were required to match the data.

The observed attenuation and the related Q of the models are the result of both anelastic absorption and scattering and/or out-of-plane lateral refraction. The possible strong effects of the latter are demonstrated by the large transverse signal generated by the air gun source in profile 2408 shown in Figure 10.

CONCLUSIONS

We have demonstrated that high-resolution longitudinal and transverse mode shear data can be obtained in shallow water regions and have derived models that agree reasonably well with independent ground truth sediment core data. Each of the four components, three sensing motion and one sensing pressure, produces unique information on wave type, velocity/attenuation structure, scattering, lateral heterogeneity, anisotropy, and instrument bottom coupling (possible signal distortion). Consequently, matching of data from all four components with synthetic data places strong constraints (i.e., greatly increases the difficulty of obtaining a satisfactory match) on the derived models. Anisotropy and lateral heterogeneity are important features of sedimentary structure and processes; they also can contribute to propagation loss. Shear data are more difficult to obtain than compressional, and horizontally polarized shear is more difficult to obtain than vertically polarized shear. However, the extra effort provides information on anisotropy and lateral refraction not available from pressure or vertical-radial motion data.

Different isotropic velocity models clearly were required to match the R-V data and the T data from profiles 2509 and 2520 near AMCOR site 6011. As discussed earlier, a single model with transverse isotropy that fits all of the data has been presented by Berge *et al.* [1991a]. For that paper the isotropic velocities provided a useful guide in the modeling. Anisotropy was suggested in other profiles, e.g., the MV profile and AGS profiles 1909 and 2113, but not clearly enough to justify the search for separate isotropic models.

The variety of measured wave field patterns shown by this study attests to the sensitivity of shear waves to changes in geological structure, and quantitative relations between the seabed structure and the wave field patterns can be determined by matching of synthetic seismograms with the recorded data. However, precise matching of waveforms and amplitudes of synthetic seismograms with field seismograms, or correlating seismic velocities with core lithology, is rarely totally successful because of the problems of matching one-dimensional model or borehole data to recorded seismic data that is sensitive to three-dimensional structure. In the AGS area particularly, information from boreholes and reflection surveys is sufficient to show that lateral structural inhomogeneity can distort wave fields even when the seismic profile lengths are only 100–200 m. The distortion can be circumvented to a large extent simply by acquiring multiple data sets to study specific targets in complex areas, but a better solution would require three-dimensional modeling.

The analyses of profiles 2509, 1909, and 2113 from the 1986 cruise have produced good matches of synthetics with recorded data for all three geophone components, even though uniqueness has not been demonstrated by formal error bounds. Data from profile 1809 and the short range data of profile 1819 were satisfactorily matched by the synthetics produced by the 1909 model. Other profiles for which data from only one or two components were acceptable, 2016 (AGS sand ridge), 2715, and 6009G (site 6009) and the ladder array data at 6010 NW produced good, although incomplete (less than three component) results. Both the geophone and accelerometer arrays determined velocity structure only to shallow depths due to the limited source-sensor ranges. However, these results have demonstrated the value of close spatial sampling at short ranges for determining the fine velocity structure in the uppermost seabed, particularly in profiles at AMCOR sites 6009G, 6009L, 6010 NW, and MV (Figures 21, 22, 24, 25, and 26).

Pressure (hydrophone) component seismograms have produced reliable depth profiles of compressional wave velocities varying from ≥ 1500 to almost 1800 m/s in the upper 5–8 m of seabed. Although the resolution of the subsurface structure with compressional waves is not as detailed as it is with shear waves, there is qualitative correspondence between the P and S results; that is, both P and S velocities are high or low, depending on the particular geological setting.

There is still much room for improvement in the instrumentation, field techniques, and data inversion. The steep gradients and short wavelengths of shear waves in the low-velocity, uppermost sediment require that sensor dimensions and spacing be small (relative to λ) for reliable results. Small SH sources need more development. Deployment of receiving arrays and shear sources on the seafloor can be difficult under conditions of adverse wind, sea, and current, particularly when the objective is to record data along specific azimuths.

Acknowledgments. Numerous people and organizations have made significant contributions to this work and it is difficult to give them all proper recognition. For the 1986 cruise, special credit is due to R. Stoll, G. Bryan, R. Flood, P. Manley, and D. Chayes, colleagues at Columbia University who were mainly responsible for shipboard data acquisition hardware and software and who provided valuable assistance on shipboard, along with R. Handy of Woods Hole Oceanographic Institution (WHOI). W. Witzell, D. DuBois, H. Hoskins, and R. Handy (WHOI) contributed significantly to the design and testing of the shear source and receiver and to data reduction. The officers and crew of R/V *Cape Henlopen* provided much helpful assistance. For the 1988 cruise, we acknowledge, again, the engineers and technicians from WHOI who provided their expertise; from Hawaii Institute of Geophysics, D. Harris, who engineered the ladder array and data acquisition system; R. Mitaguy, who was responsible for mechanical components of the ladder array; P. Berge, graduate student on the project; and the officers and crew of R/V *Oceanus* who provided essential assistance for successful deployment of the ladder array. We wish to thank internal reviewers D. G. Aubrey, C. O. Bowin, and S. D. Rajan and external reviewers L. M. Dorman, A. M. Trehu, and T. Yamamoto for helpful suggestions that significantly improved this contribution. Finally, we gratefully acknowledge support of this research by the Office of Naval Research under an Accelerated Research Initiative monitored by J. H. Kravitz (contract N00014-88-C-0238).

REFERENCES

- Akal, T., Sea floor effects on shallow-water acoustic propagation, in *Bottom-Interacting Ocean Acoustics*, edited by W. A. Kuperman and F. B. Jensen, *NATO Conf. Ser. 4, 5*, 557–575, 1980.
- Beebe, J. H., and C. W. Holland, The effect of unconsolidated sediment rigidity on low frequency acoustic propagation, in *Ocean Seismo-Acoustics Low Frequency Underwater Acoustics*, edited by T. Akal and J. M. Berkson, *NATO Conf. Ser. 4, 16*, 207–216, 1986.
- Berge, P. A., Estimating SV-wave stacking velocities for transversely isotropic solids, *Geophysics*, **5**, 1596–1602, 1991.
- Berge, P. A., S. Mallick, G. J. Fryer, N. Barstow, J. A. Carter, G. H. Sutton, and J. I. Ewing, In situ measurement of transverse isotropy in shallow-water marine sediments, *Geophys. J. Int.*, **104**, 241–254, 1991a.
- Berge, P. A., S. Mallick, G. J. Fryer, N. Barstow, J. A. Carter, G. H. Sutton, and J. I. Ewing, Refraction measurement of shear wave anisotropy in shallow marine sediments and implications for reflection processing, in *Shear Waves in Marine Sediments*, edited by J. M. Hovem, M. D. Richardson, and R. D. Stoll, pp. 203–212, Kluwer Academic, Boston, Mass., 1991b.
- Biot, M. A., A generalized theory of acoustic propagation in porous dissipative media, *J. Acoust. Soc. Am.*, **34**, 1254–1265, 1962.
- Bothner, M. H., E. Spiker, W. Ferrebee, and D. Peeler, Texture, clay mineralogy, trace metals, and age of cored sediments from the North Atlantic outer continental shelf, *U.S. Geol. Surv. Open File Rep.*, 79–842, 41 pp., 1979.
- Bucker, H. P., J. A. Whitney, and D. L. Keir, Use of Stoneley waves to determine the shear velocity in ocean sediments, *J. Acoust. Soc. Am.*, **36**, 139–143, 1964.
- Carter, J. A., G. H. Sutton, and N. Barstow, Synthetic modeling of shear waves in shallow marine sediments (abstract), *J. Acoust. Soc. Am.*, **82**, S112, 1987.
- Clayton, R. W., and G. A. McMechan, Inversion of refraction data by wave field continuation, *Geophysics*, **46**, 860–868, 1981.
- Crampin, S., Evaluation of anisotropy by shear-wave splitting, *Geophysics*, **50**, 142–152, 1985.
- Dames and Moore, Supplementary subsurface investigation: Vibration program, Atlantic Generating Station, Public Serv. Elect. and Gas Co., Newark, N. J., 1974.
- Davies, D., Dispersed Stoneley waves on the ocean bottom, *Bull. Seismol. Soc. Am.*, **55**, 903–918, 1965.
- Davies, T. A., J. A. Austin, Jr., M. B. Lagoe and J. D. Milliman, Late Quaternary sedimentation off New Jersey: New results using 3-D seismic profiles and cores, *Mar. Geol.*, in press, 1992.
- Dorn, G. A., Radiation pattern of torsionally vibrating sources, *Geophysics*, **99**, 1213–1222, 1984.
- Essen, H. H., Model computations for low-velocity surface waves on marine sediments, in *Bottom-Interacting Ocean Acoustics*, edited by W. A. Kuperman and F. B. Jensen, *NATO Conf. Ser. 4, 5*, 299–305, 1980.
- Ferla, M. C., G. Dreini, F. B. Jensen, and W. A. Kuperman, Broadband model-data comparisons for acoustic propagation in coastal waters, in *Bottom-Interacting Ocean Acoustics*, edited by W. A. Kuperman and F. B. Jensen, *NATO Conf. Ser. 4, 5*, 577–592, 1980.
- Fryer, G. J., and D. J. Miller, Effects and consequences of transverse isotropy in the seafloor, in *Ocean Seismo-Acoustics Low Frequency Underwater Acoustics*, edited by T. Akal and J. M. Berkson, *NATO Conf. Ser. 4, 16*, 589–598, 1986.
- Gehrmann, T., P. Gimpel, and F. Theilen, Marine shear wave profiling, paper presented at 54th Annual International Meeting, Soc. of Exp. Geophys., Atlanta, Ga., Dec. 3–6, 1984.
- Gupta, I. N., and R. R. Blandford, A mechanism for generation of short-period transverse motions from explosions, *Bull. Seismol. Soc. Am.*, **73**, 571–591, 1983.
- Hamilton, E. L., Shear-wave velocity versus depth in marine sediments: A review, *Geophysics*, **41**, 985–996, 1976a.
- Hamilton, E. L., Attenuation of shear waves in marine sediments, *J. Acoust. Soc. Am.*, **60**, 334–338, 1976b.
- Hamilton, E. L., V_p/V_s and Poisson's ratios in marine sediments and rocks, *J. Acoust. Soc. Am.*, **66**, 1093–1101, 1979.
- Hamilton, E. L., Geoaoustic modeling of the sea floor, *J. Acoust. Soc. Am.*, **68**, 1313–1340, 1980.
- Harris, D., and G. H. Sutton, Soft sediment shear wave sensor string, *Eos Trans. AGU*, **69**, 1319, 1988.
- Harvey, D. J., Seismogram synthetics using normal mode superposition: The locked mode approximation, *Geophys. J. R. Astron. Soc.*, **65**, 682–686, 1981.
- Hathaway, J. C., et al., Preliminary summary of the 1976 Atlantic

- Margin Coring Project of the U.S. Geological Survey, *U.S. Geol. Surv. Open File Rep.*, 76-844, 217 pp., 1976.
- Hawker, K. E., The existence of Stoneley waves as a loss mechanism in plane wave reflection problems, *J. Acoust. Soc. Am.*, 65, 682-686, 1979.
- Hsieh, T. K., Foundation vibrations, *Proc. Inst. Civ. Eng.*, 22, 211-266, 1962.
- Hughes, S. J., D. D. Ellis, D. M. F. Chapman, and P. R. J. Staal, Low-frequency acoustic propagation loss in shallow water over hard-rock seabeds covered by a thin layer of elastic-solid sediment, *J. Acoust. Soc. Am.*, 88, 283-297, 1990.
- Jensen, F. B., and H. Schmidt, Shear properties of ocean sediments determined from numerical modelling of Scholte wave data, in *Ocean Seismo-Acoustics Low Frequency Underwater Acoustics*, edited by T. Akal and J. M. Berkson, *NATO Conf. Ser. 4*, 16, 683-692, 1986.
- Kisslinger, C., E. J. Mateker, Jr., and T. V. McEvilly, SH motion from explosions in soil, *J. Geophys. Res.*, 66, 3487-3496, 1961.
- Lash, C. C., Shear waves, multiple reflections, and converted waves found by a deep vertical wave test (vertical seismic profiling), *Geophysics*, 45, 1373-1411, 1980.
- Mallick, S., and L. N. Frazer, Rapid computation of multi-offset vertical seismic profile synthetic seismograms for layered media, *Geophysics*, 53, 479-491, 1988.
- Mallick, S., and L. N. Frazer, Computation of synthetic seismograms for stratified azimuthally anisotropic media, *J. Geophys. Res.*, 95, 8513-8526, 1990.
- McDaniel, S. T., and J. H. Beebe, Influence of semiconsolidated sediments on sound propagation in a coastal region, in *Bottom-Interacting Ocean Acoustics*, edited by W. A. Kuperman and F. B. Jensen, *NATO Conf. Ser. 4*, 5, 493-505, 1980.
- McMechan, G. A., and M. J. Yedlin, Analysis of dispersive waves by wave field transformation, *Geophysics*, 46, 869-874, 1981.
- Meissner, R., H. Stümpel, and F. Theilen, Shear wave studies in shallow sediments, in *Handbook of Geophysical Exploration*, edited by G. Dohr, pp. 224-253, Geophysical Press, London, 1985.
- Milholland, P., M. H. Manghnani, S. O. Schlanger, and G. H. Sutton, Geoacoustic modeling of deep-sea carbonate sediments, *J. Acoust. Soc. Am.*, 68, 1351-1360, 1980.
- Miller, H. J., and C. Dill, Final report, Geophysical investigations of Atlantic Generating Station and Offshore Region, Public Serv. Electr. and Gas Co., Newark, N.J., 1974.
- Milliman, J. D., J. Z. Zhaung, A. C. Li, and J. I. Ewing, Late Quaternary sedimentation on the outer and middle New Jersey continental shelf: Result of two local deglaciations?, *J. Geol.*, 98, 966-976, 1990.
- Morton, R. A., Late Quaternary geology of the Texas coastal plain, in *Centennial Field Guide*, vol. 4, *South-Central Section*, edited by O. T. Hayward, pp. 445-458, Geological Society of America, Boulder, Colo., 1988.
- Nettleton, L. L., *Geophysical Prospecting for Oil*, 444 pp., McGraw-Hill, New York, 1940.
- Ohsaki, Y., and R. Iwasaki, On dynamic shear moduli and Poisson's Ratios of soil deposits, *J. Soils Found. Jpn. Soc. Soil Mech. Found. Eng.*, 13(4), 61-73, 1973.
- Rajan, S. D., and C. S. Howitt, Determination of the sediment shear speed profiles from phase and group velocity dispersion data of SH wave, in *Shear Waves in Marine Sediments*, edited by J. M. Hovem, M. D. Richardson, and R. D. Stoll, pp. 529-536, Kluwer Academic, Boston, Mass., 1991.
- Rauch, D., Experimental and theoretical studies of seismic interface waves in coastal waters, in *Bottom-Interacting Ocean Acoustics*, edited by W. A. Kuperman and F. B. Jensen, *NATO Conf. Ser. 4*, 5, 285-298, 1980.
- Rauch, D., On the role of bottom interface waves in ocean seismo-acoustics: A review, in *Ocean Seismo-Acoustics Low Frequency Underwater Acoustics*, edited by T. Akal and J. M. Berkson, *NATO Conf. Ser. 4*, 16, 623-642, 1986.
- Richards, A. F., Atlantic Margin Coring Project 1976: Preliminary report on shipboard and some laboratory geotechnical data, *U.S. Geol. Surv. Open File Rep.*, 78-123, 1977.
- Sauter, A. W., L. M. Dorman, and A. E. Schreiner, A study of sea floor structure using ocean bottom shots and receivers, in *Ocean Seismo-Acoustics Low Frequency Underwater Acoustics*, edited by T. Akal and J. M. Berkson, *NATO Conf. Ser. 4*, 16, 673-681, 1986.
- Schirmer, F., Experimental determination of properties of the Scholte wave in the bottom of the North Sea, in *Bottom-Interacting Ocean Acoustics*, edited by W. A. Kuperman and F. B. Jensen, *NATO Conf. Ser. 4*, 5, 285-298, 1980.
- Schmalfeldt, B., A comparison of seismic and hydroacoustic measurements at very low frequencies in different shallow water areas, in *Ocean Seismo-Acoustics Low Frequency Underwater Acoustics*, edited by T. Akal and J. M. Berkson, *NATO Conf. Ser. 4*, 16, 653-662, 1986.
- Schreiner, A. E., and L. M. Dorman, Coherence lengths of seafloor noise: Effect of ocean bottom structure, *J. Acoust. Soc. Am.*, 88, 1503-1514, 1990.
- Snoek, M., G. Guidi, and E. Michelozzi, Interface wave studies on the Ligurian shelf using an OBS array: Experimental results and propagation models, in *Ocean Seismo-Acoustics Low Frequency Underwater Acoustics*, edited by T. Akal and J. M. Berkson, *NATO Conf. Ser. 4*, 16, 663-672, 1986.
- Stahl, L., J. Koczan, and D. Swift, Anatomy of a shoreface-connected sand ridge on the New Jersey shelf: Implications for the genesis of the shelf surficial sand sheet, *Geology*, 2, 117-120, 1974.
- Stern, M., A. Bedford, and H. R. Millwater, Wave reflection from a sediment layer with depth-dependent properties (abstract), *J. Acoust. Soc. Am.*, 74, suppl. 1, 543, 1983.
- Stickler, D. C., Measurement of the sound speed in bottom layers, *J. Acoust. Soc. Am.*, 57, 585-590, 1975.
- Stoll, R. D., Theoretical aspects of sound transmission in sediments, *J. Acoust. Soc. Am.*, 68, 1341-1350, 1980.
- Stoll, R. D., Sediment acoustics, V, *Lect. Notes Earth Sci.*, 26, 155 pp., 1989.
- Stoll, R. D., G. M. Bryan, R. Mithal, and R. Flood, Field experiments to study seismoacoustic response, *J. Acoust. Soc. Am.*, 89, 2232-2240, 1991.
- Sutton, G. H., and F. K. Duennebie, Optimum design of ocean bottom seismometers, *Mar. Geophys. Res.*, 9, 47-65, 1987.
- Trevorrow, M. V., and T. Yamamoto, Summary of marine sedimentary shear modulus and acoustic speed profile results using a gravity wave inversion technique, *J. Acoust. Soc. Am.*, 90, 441-456, 1991.
- Trevorrow, M., T. Yamamoto, M. Badiy, A. Turgut, and C. Conner, Experimental verification of sea-bed shear modulus profile inversions using surface gravity (water) wave-induced sea-bed motion, *Geophys. J.*, 93, 419-436, 1988.
- Twichell, D. C., C. E. McClennen, and B. Butman, Morphology and processes associated with the accumulation of the fine-grained sediment deposit on the southern New England shelf, *J. Sediment. Petrol.*, 51, 0269-0280, 1981.
- Vidmar, P. J., The effect of sediment rigidity on bottom reflection loss in a typical deep sea sediment, *J. Acoust. Soc. Am.*, 68, 634-638, 1980a.
- Vidmar, P. J., Ray path analysis of sediment shear wave effects on bottom reflection loss, *J. Acoust. Soc. Am.*, 68, 639-648, 1980b.
- Vidmar, P. J. and R. A. Koch, Shear wave effects on propagation to a receiver in the substrate, in *Ocean Seismo-Acoustics Low Frequency Underwater Acoustics*, edited by T. Akal and J. M. Berkson, *NATO Conf. Ser. 4*, 16, 149-158, 1986.
- White, J. E., *Seismic Waves*, McGraw-Hill, New York, 1965.
- Yamamoto, T., and T. Torii, Seabed shear modulus profile inversion using surface gravity (water) wave-induced bottom motion, *Geophys. J. R. Astron.*, 85, 413-431, 1986.
- Yamamoto, T., M. V. Trevorrow, M. Badiy, and A. Turgut, Determination of the seabed porosity and shear modulus profiles using a gravity wave inversion, *Geophys. J. Int.*, 98, 173-182, 1989.
- N. Barstow, 39 Piermont Place, Piermont, NY 10968.
- J. A. Carter, Center for Seismic Studies, SAIC, 1300 N 17th St., Suite 1450, Arlington, VA 22209.
- J. Ewing and G. H. Sutton, Department of Geology and Geophysics, Woods Hole Oceanographic Institution, Woods Hole, MA 02543.

(Received August 7, 1991;
accepted November 21, 1991.)